Molecular Regulation of Arp2/3 Complex Branch Nucleation in Assembly of Actin Networks

by

Sofia Rebecka Carlson

A dissertation accepted and approved in partial fulfillment of the

requirements for the degree of

Doctor of Philosophy

in Chemistry

Dissertation Committee:

Scott Hansen, Chair

Brad Nolen, Advisor

Ken Prehoda, Core Member

Diane Hawley, Core Member

Bruce Bowerman, Institutional Representative

University of Oregon

Fall 2025

DISSERTATION ABSTRACT

Sofia Rebecka Carlson

Doctor of Philosophy in Chemistry

Title: Molecular Regulation of Arp2/3 Complex Branch Nucleation in Assembly of Actin Networks

The Arp2/3 complex is a key actin filament nucleator responsible for the formation of force producing branched actin networks. Determining how it is activated and regulated is critical for understanding how force production drives dynamic cellular processes such as motility and endocytosis. Intrinsically inactive, the Arp2/3 complex must bind activators to adopt a short pitch, flattened conformational state. Nucleation of linear filaments occurs when activated by a member of the WISH/DIP/SPIN90 (WDS) family of proteins while nucleation of branched filaments requires a member of the WASP family of proteins, monomer recruitment by WASP, and a preformed actin filament. The role of each activator in stimulating these conformational changes and activating the Arp2/3 complex during branch nucleation remains unclear. We show that monomer recruitment is required specifically for the WASP-mediated mechanism but is not a fundamental requirement for human Arp2/3 complex activation. WASP and WASP-tethered monomers stimulate the short pitch state but can be bypassed in splayed interface mutant complexes that more readily adopt the short pitch state. Formation of a filament nucleus from which elongation proceeds can occur without direct monomer tethering via monomer collisions. Though splayed interface mutants bypass WASP and WASP-mediated monomer recruitment *in vitro*, they cause only minor defects in cellular actin networks in *Saccharomyces cerevisiae.* Mutants show increased actin accumulation and longer actin lifetimes, indicating a change in network architecture, but endocytic internalization proceeds normally. These observations

suggest additional unexplored mechanisms control the regulation of the Arp2/3 complex in vivo. We show that the Arp2/3 complex has intrinsically disordered regions (IDRs) located at its filament binding surface that are important for full nucleation activity. Analysis of these IDRs and design of high-affinity actin filament binding mutants will be an important future step in determining the influence of filament binding in targeting Arp2/3 complex to the membrane. This work has clarified the mechanisms of Arp2/3 complex activation and its regulation within polarized, functional actin networks, contributing to our understanding of actin nucleation and assembly.

This dissertation includes previously published and unpublished co-authored material.

CURRICULUM VITAE

NAME OF AUTHOR: Sofia Rebecka Carlson

GRADUATE AND UNDERGRADUATE SCHOOLS ATTENDED:

University of Oregon, Eugene
University of Wisconsin-Madison, Madison, WI

DEGREES AWARDED:

Doctor of Philosophy, Chemistry and Biochemistry, 2025, University of Oregon
Bachelor of Science, Biochemistry, 2016, University of Wisconsin-Madison

AREAS OF SPECIAL INTEREST:

Biochemistry
Molecular Biology
Biophysics

PROFESSIONAL EXPERIENCE:

Graduate Research Fellow, Department of Chemistry and Biochemistry
University of Oregon, Eugene, OR, 2020-2025

Graduate Teaching Fellow, Department of Biology
University of Oregon, Eugene, OR, 2025

Graduate Teaching Fellow, Department of Chemistry and Biochemistry
University of Oregon, Eugene, OR, 2020-2021, 2024

Biochemist, Associate Biochemist, Kendrick Laboratories
Madison, WI, 2016-2020

GRANTS, AWARDS, AND HONORS:

NIH T32 Molecular Biology and Biophysics Training Program, University of Oregon, 2021-2022
Stanley David and Lucille Borgen Adamson Memorial Award, University of Oregon, 2021

Graduate Student Award for Excellence in the Teaching of Chemistry, University Oregon, 2021

Dean's First Year Merit Award, University of Oregon, 2020

PUBLICATIONS:

Carlson S. and Nolen B. Direct actin monomer delivery is a WASP-specific requirement for human Arp2/3 complex activation. *Journal of Molecular Biology*. (Submitted). (2025).

Kendrick, N., Powers, G., Johansen, J., Hoelter, M., Koll, A., **Carlson, S.**, Channaveerappa, D., Darie, C.C., 2020. Preparation of a phosphotyrosine-protein standard for use in semiquantitative western blotting with enhanced chemiluminescence. *PLoS One* **15**, (2020).

ACKNOWLEDGMENTS

First and foremost, I would like to thank my advisor Dr. Brad Nolen for his support throughout my time here, helping me become a better scientist. His excitement for science and perfectly timed pep talks did wonders for my motivation during the most difficult experimental failures. I would also like to thank my committee members Dr. Scott Hansen, Dr. Ken Prehoda, Dr. Diane Hawley, and Dr. Bruce Bowerman, who offered great advice and support.

To the various members of the Nolen lab over the years, I've loved the perfect balance of work and fun that I found in our lab. I especially want to thank Dr. Heidy Narvaez-Ortiz, the only member of the lab who has been with me since the beginning, and a stellar scientist. I have learned a great deal of protein biochemistry in our many discussions and am lucky to have had such a knowledgeable and kind person in the lab with me my entire time here. To Dr. Mike Lynch, Dr. Vignesh Ravichandran, Dr. Mousumi Akter, Dr. Brody Bills, Maisie Topping, Peter Lechman, Charlotte DiGaetano, and Michelle Ortman, I thank you for all the chit-chatting and laughter you brought to our workspace. Thank you to Stu Johnson and Adam Fries for your knowledge and support and to Dr. Parisa Hosseinzadeh for your help learning Rosetta.

The community I have found at the University of Oregon helped me through all the long days and failed protein purifications. To the Hansen lab, especially Dr. Benjamin Duewell, Sophia Doerr, and Emma Drew, who welcomed me with open arms when I wanted grad students to commiserate with, I thank you for letting me be an honorary member of your lab. The friendships that developed out of those initial biochemistry hang outs (including Anthony and Luci!) have supported me through the highs and the lows of grad school. I thank the Abcam friends for welcoming me and letting me get out of my grad school bubble. To Dr. Julia Ngo, Sam Horst, Jordan Brown, Addison Dobias, and Dr. Kona Shaw, I thank each of you for all the

talks about everything and nothing. To the Sophfias (Sophia Doerr and Dr. Sophia Phillips), I am so happy that our shared names allowed for the formation of genuine friendships.

Thank you to the friends who've been there since the beginning. To Alyssa Quiogue, who rotated in the Nolen Lab with me and introduced me to Lucy Moholt-Siebert, having you both as our first "couple friends" has been a blast for Beth and me. Thank you for all the food, watch parties, gaming, Dr. Peppers, laughter, and love. To the very first person I met at UO, Emily Dennis, I knew you were going to be my friend immediately, but I didn't know just how much support you would give me in my time here. I am forever grateful for all the science chats, life chats, and food we have shared. Thank you to you and Max Horrocks for letting me pursue my hobbies in your home while giving me all the hype.

To my Mom, Lena, and Britta, though I have missed you all dearly, the daily pings of our group chat have made me feel like you aren't across the country. Thank you for cheering me on and believing in me, even when you had no idea what I was doing. I treasure the times I have had in-person with all of you, Bob, and Jake, and look forward to more antics.

Finally, I thank the person who was my biggest rock through this journey, my wife, Beth Scholze. She moved across the country during COVID with me and our two baby kitties, Owl and Ripley, to begin this grand adventure and planned a wedding with me mid-way through grad school. I couldn't have made it to the end without the unconditional love of this little family. Thank you for being my home during the happiest and hardest of times. I'm excited for the next chapter of our lives!

This work was funded by the Molecular Biology and Biophysics Training Grant (5T32GM007759) and Dr. Brad Nolen's MIRA (R35GM136319).

DEDICATION

I dedicate this dissertation to my wife, kitties, friends, and family who provided the love and support I needed on this journey.

TABLE OF CONTENTS

LIST OF FIGURES

Figure Page

LIST OF TABLES

Table Page

CHAPTER ONE

INTRODUCTION

The Role of the Actin Cytoskeleton in Cells

Cells carry out a variety of complex processes such as endocytosis, cell division, cell motility, DNA repair, phagocytosis, and tissue morphogenesis that are inherently dynamic[1–6]. For example, during motility, broad protrusions called lamellipodia extend forward and adhere to an extracellular substrate, driving the cell forward. Membrane dynamics are critical for endocytosis during which membrane invagination allows for internalization of extracellular cargoes, critical for nutrient uptake and cellular signaling. At a broader scale, changes in cell shape drive tissue morphogenesis during development. These dynamic processes are all driven by the production of force that requires precise spatiotemporal coordination.

Cells produce force for diverse functionalities through the machinery of a vast cytoskeletal network. The cytoskeleton consists of polymers of filaments and microtubules composed of monomers of actin and dimers of tubulin respectively. Upon polymerization, microtubules and crosslinked actin filaments provide a stiffness that is critical for maintenance of structural integrity in cells[7,8]. At the cell cortex, a dense network of actin filaments, actin binding proteins and myosin about 200 nm thick, provides surface tension that resists external forces, while also producing contractile forces, allowing for changes in cell shape [9–12]. Though previously believed to belong to distinct cytoskeletal networks, growing evidence has suggested a role for actin-microtubule crosstalk[13]. Additionally, microtubules have been shown to promote cortical stiffness that counteracts actomyosin contractility[14]. The ability of these polymers to depolymerize and repolymerize allows them to respond to signaling cues or external forces accordingly.

The polymerization of actin into filaments occurring during assembly of dendritic networks is a ubiquitous, highly regulated process. Actin is one of the most abundant proteins in eukaryotic cells, with total concentrations estimated to be in the range of 12-300 μM and local concentrations of actin filaments estimated to be in the range of 500 to 1600 μM[15–19]. Net growth of actin networks occurs when monomer concentrations are above the "critical concentration" of 0.1 μM where polymerization and depolymerization are in equilibrium[15]. Network assembly is further regulated by a variety of proteins that interact with actin in its monomeric or filamentous form, influencing filament nucleation, stabilization, and disassembly. These regulatory mechanisms allow the same machinery to be used in a variety of processes.

The actin cytoskeleton plays a critical role in dynamic force production in cells. Filaments are incorporated into polarized networks that are assembled and disassembled rapidly, on the order of seconds in lamellipodia[20]. As a single filament polymerizes, monomers are added to the rapidly growing end, producing a pushing force of 1-2 pN[21,22]. When many filaments elongate concurrently in vast networks, the total force produced is compounded, producing estimated forces of 1000-2500 pN/μm^2 [17,23]. The extent of this force production depends on the organization of the actin networks.

The architecture of an actin network influences its force production and functionality. Networks differ in filament density and relative abundance of branched versus linear filaments. Cellular networks adapt to differences in mechanical load by changing filament density, allowing denser actin networks to produce increased force against greater loads[24,25]. Branched actin networks are utilized in processes that require greater pushing forces. They are found in broad, flat lamellipodial protrusions that are optimal for pushing on the membrane during cellular

motility and at endocytic patches where the spatial organization at the base of the invagination site is optimal for production of pushing and pulling forces that create and internalize a vesicle[26,27]. Linear filaments are found primarily in filopodia, thin finger-like protrusions, where they are aligned and bundled, producing weaker forces[21] but faster overall growth of the structure[28], important for sensing and exploring their environment [29]. The organization of actin into branched and linear architectures depends on the regulation of actin nucleation and assembly.

Mechanism of Actin Nucleation

The assembly of actin networks depends on the structural properties of actin. Actin monomers are 42 kDa globular proteins consisting of four subdomains forming an outer (subdomains 1 and 2) and inner (subdomains 3 and 4) domain[30]. Two grooves lie between the outer and inner domains; at the pointed end of the monomer is the nucleotide binding pocket (between subdomains 2 and 4) which binds ATP and cations (Mg^{2+} in cells), and at the barbed end of the monomer is the barbed end groove (between subdomains 1 and 3), a common binding target[31]. Actin transitions between its globular monomeric form, its G-state, to its filamentous form, its F-actin state, in which each monomer adopts a flattened conformation through the rotation of the outer domain relative to the inner domain[32,33]. The filamentous form consists of a single left-handed helix resembling two right-handed helical strands in which consecutive actin subunits bind along the short pitch helical axis[33]. During polymerization, a DNaseI-loop (D-loop) on subdomain 2 at the pointed end of each subunit inserts itself into the barbed end groove at the barbed end of an adjacent, longitudinal subunit[34]. This directionality results in a filament containing a fast-growing barbed (+) end and a slow-growing pointed (-) end, which elongate at

steady rates, 11.6 and 1.3 $\mu M^{-1}s^{-1}$ respectively[35]. Before elongation can proceed, however, an unfavorable nucleation step must occur. Spontaneous nucleation involves the formation of an actin nucleus, a stable oligomer from which elongation can occur. Actin monomers diffuse and collide to form dimers, trimers, and tetramers, with the nucleus likely formed upon trimer or tetramer assembly[36]. Because spontaneous nucleation is a slow, unfavorable process, cells rely on actin filament nucleators to lower the energy barrier of nucleation. These include formins, tandem WH2 domains, and the Arp2/3 complex.

Nucleators of linear actin filaments function by recruiting monomers to form a nucleus or by structurally mimicking actin subunits within a filament. Formins are a large family of dimeric proteins involved in processive elongation and nucleation of linear filaments. They are characterized by the presence of proline-rich formin-homology 1 (FH1) and formin-homology 2 (FH2) domains. The FH2 domains have a donut-like structure that allows them to processively bind to the barbed end of actin filaments and incorporate actin monomers to regulate elongation[37]. As FH2 domains show no affinity for actin monomers, nucleation is thought to occur via stabilization of actin dimers or trimers[38] and recruitment of actin monomers via regions at the C-terminus[39,40]. Proteins containing tandem WASP-homology 2 (WH2) domains such as JMY[41], Spire[42], and Cobl[43] bind actin monomers at each domain, recruiting multiple monomers for nucleus formation. The number of WH2 domains and length of linkers, which differs between proteins, determines the positioning of the monomers by influencing formation of longitudinal and lateral contacts, likely influencing nucleation activity[44]. An alternative nucleation pathway is carried out by the Arp2/3 complex, which can nucleate linear filaments by mimicking a filamentous actin dimer when activated by a member of the WISH/DIP/SPIN90 (WDS) family of proteins[45]. The linear filaments created by unique nucleators are bundled and

assembled into actin structures such as filopodia, actin cables, cytokinetic rings, and stress fibers[46].

Arp2/3 Complex Nucleation of Branched Actin Filaments

The only known nucleator of branched actin filaments is the Arp2/3 complex. This complex was first purified and characterized from *Acanthamoeba castellanii*[47,48], but is well conserved across diverse eukaryotic species[49] and has since been purified and characterized from *Saccharomyces cerevisiae*[50], *Schizosaccharomyces pombe*[51,52], *Bos taurus*[53], and humans[49]. Its presence is essential as evidenced by the lethality of deletions of genes encoding individual subunits of the complex in *S. pombe* or *S. cerevisiae*[50,51,54,55] and inability to obtain viable Arp3, Arp2, or ARPC1 null mouse embryo fibroblast cell lines without additional modifications [56,57]. Additionally, it has been shown to have critical roles in lamellipodia[58–60], endocytosis[61–63], focal adhesions[64], and DNA repair[65].

The Arp2/3 complex consists of seven subunits, including actin related proteins (Arps) Arp2 and Arp3, and the scaffolding proteins ARPC1, ARPC2, ARPC3, ARPC4, and ARPC5. Evidence of its branch nucleation activity was first observed by electron microscopy showing the complex bound to the side of a "mother" actin filament and the pointed end of a "daughter" filament, forming a branch junction at a consistent 70° angle[66]. Arp2 and Arp3 were named actin related proteins due to their high sequence similarity to actin, believed fundamental to their influence on actin assembly[67]. A high resolution structure of Arp2/3 complex confirmed that the Arp subunits had high structural similarity to that of monomeric actin[53], though with insertions that have since been characterized in yeast[68]. The high sequence and structural similarity to actin suggested that Arp2/3 complex was able to template a branch by mimicking an actin dimer.

To mimic a filamentous actin dimer, the Arp2/3 complex must adopt a short pitch, flattened conformation (Figure 1.1A and 1.1B). The short pitch conformation mimics the arrangement of two consecutive actin subunits within the short pitch helical axis of an actin filament whereas flattening corresponds to the conformational change that occurs within an actin monomer during polymerization[33,69–79]. Low resolution reconstructions and structures of Arp2/3 complex at the branch junction[75,80] and subsequent high-resolution structures of active Arp2/3 complex[77–79,81] observe Arp2 and Arp3 in this short pitch, flattened state. These high-resolution structures have clarified the conformational changes occurring as the complex moves from the inactive to the active state. The splayed to short pitch transition occurs via a large rigid body movement of ARPC1, ARPC5, Arp2, and a portion of ARPC4, initiated by twisting of an ARPC2 and ARPC4 clamp, which moves Arp2 relative to Arp3, creating a short pitch Arp heterodimer (Figure 1.1C)[76,78] . Movement of Arp2 out of the inactive, splayed state frees the barbed end of Arp3 for the incoming actin monomer of the daughter filament. In addition to the inter-subunit movements, intra-subunit flattening occurs in both Arp2 and Arp3 as their outer domain (subdomains 1 and 2) rotates relative to their inner domain (subdomains 3 and 4), analogous to the twisted to flattened transition each actin subunit undergoes during polymerization (Figure 1.1D and 1.1E)[76,77]. This includes a widening of their barbed end grooves, allowing for the insertion of incoming actin D-loops. Flattening in Arp3 also brings it closer to the mother filament, increasing contacts and buried surface area[82]. Additionally, flattening is believed to prime the Arps for ATP hydrolysis[76,77,82], important for branch disassembly and network recycling[83,84]. Activators of Arp2/3 complex must induce the short pitch and flattened confirmational changes to produce a nucleation competent state.

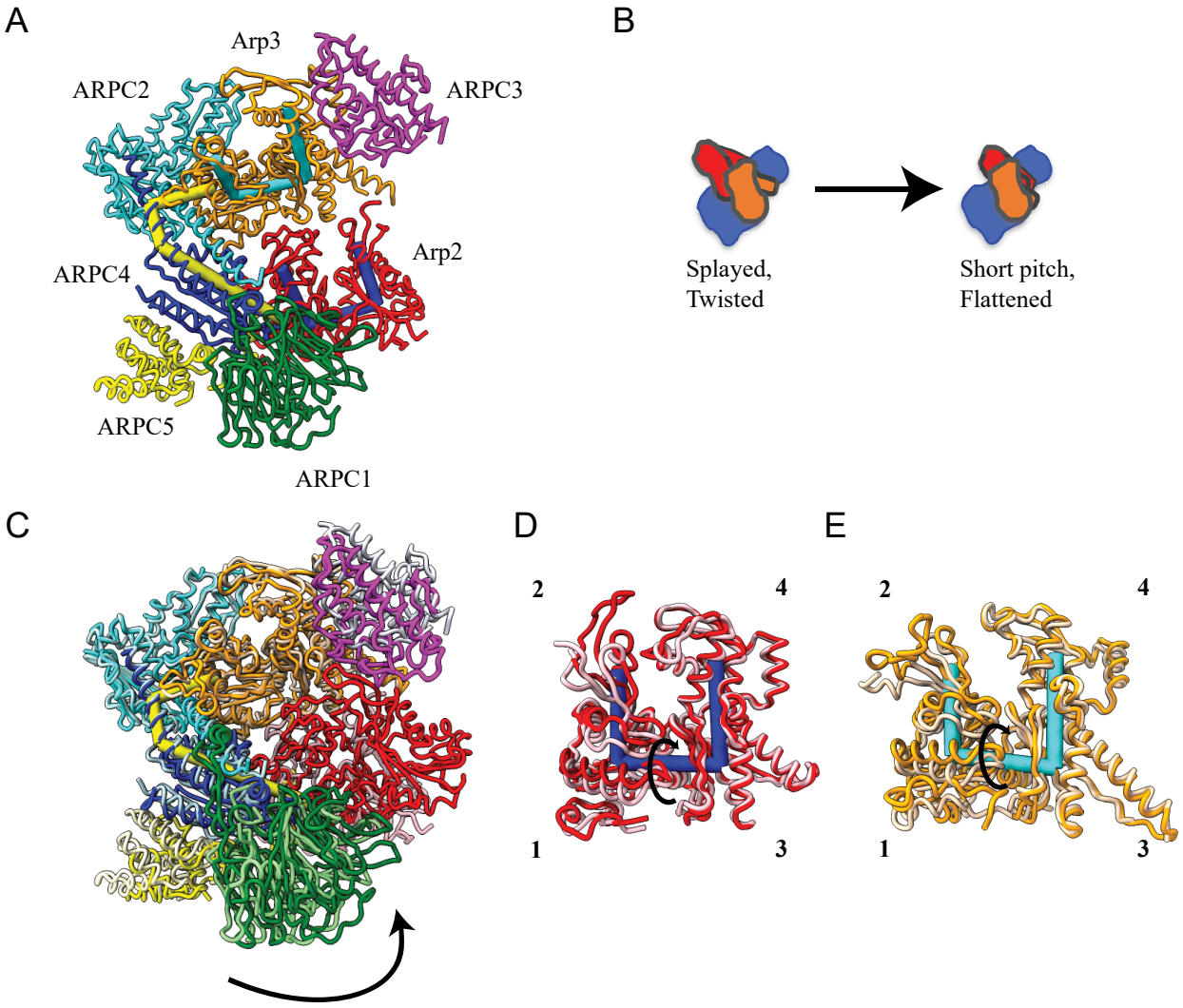

Figure 1.1. Activating conformational changes in the Arp2/3 complex. A) Structure of the inactive Arp2/3 complex (PDB: 4jd2) in the splayed, twisted conformation. Yellow dihedral indicates clamp twisting during splayed to short pitch transition. Blue and cyan dihedrals indicate location of flattening in Arp2 and Arp3. B) Cartoon representing the activating conformational changes in the Arp2/3 complex. C) Structure of the active Arp2/3 complex (PDB: 7tpt) overlaid over its inactive state (in light colors, PDB: 4jd2). Yellow dihedral indicates clamp twisting. Arrow shows the direction of movement during the splayed to short pitch transition. D) Active Arp2 overlaid with inactive Arp2 (light red). Dihedral is measured as the center of mass between the 4 subdomains. Arrow indicates movement of subdomains 1 and 2 during flattening. E) Active Arp3 overlaid with inactive Arp2 (light orange). Dihedral is measured as the center of mass between the 4 subdomains. Arrow indicates movement of subdomains 1 and 2 during flattening.

The Arp2/3 complex is intrinsically inactive and requires activating proteins to overcome the energy barrier between the stable inactive state and the high energy active state. During branch nucleation, the complex must bind to a preformed actin filament, a nucleation promoting factor such as a member of the WASP family of proteins, and actin monomers recruited by WASP[85,86]. These activators drive the conformational changes required for Arp2/3 complex activation, providing a key regulatory role in the assembly of actin networks.

Regulators of the Arp2/3 Complex

The primary regulators of the Arp2/3 complex are nucleation promoting factors, or NPFs, which are typically sorted into two groups: type I (WASP), which bind to Arp2/3 complex and actin monomers, and type II (cortactin), which bind to Arp2/3 complex and actin filaments. WDS proteins have formed a class of their own as they have not been shown to interact with actin monomers or filaments and thus activate the complex through a distinct mechanism to nucleate linear filaments.

Type I NPFs such as WASP, N-WASP, WAVE, WHAMM, and WHIMP are characterized by the presence of a verprolin-homology, central, and acidic (VCA) sequence[87]. WASP proteins also form a number of protein interactions through proline-rich regions, acting as a signaling module for Arp2/3 complex activation[88]. The verprolin-homology (V) or WH2 domain binds to actin monomers with low micromolar to nanomolar affinity and recruits actin monomers to the complex[85,89–91]. The disordered CA motif binds the Arp2/3 complex in one of two sites: on Arp3 or spanning Arp2 and ARPC1[80–85]. Upon binding, the C region forms an amphipathic helix and the A region becomes partially ordered[74,92]. The C helix binds in the barbed end groove of Arp2 and Arp3, a site that overlaps with the location of the D-loop of the

incoming actin monomer. Consequently, WASP also plays an inhibitory role, supported by the observation that it must be released prior to branch nucleation[93]. Biochemical experiments investigating the role of WASP in the Arp2/3 complex activation mechanism have found that WASP stimulates adoption of the short pitch conformation[70,73,74,94]. The requirement for WASP in this activating conformational change ensures branch nucleation is spatially controlled, though the influence of the splayed to short pitch equilibrium in regulating functional cellular actin networks is unknown. Polybasic regions in WASP interact with phosphoinositide lipids, resulting in WASP localization to the membrane[95]. This ensures Arp2/3 complex is activated at the membrane, producing a polarized actin network capable of force production.

In the WASP-mediated activation mechanism, direct actin monomer tethering is necessary for optimal branch nucleation by the Arp2/3 complex. WASP constructs containing the CA motif but lacking the WH2 domain stimulate the short pitch state but fail to potently activate the Arp2/3 complex[70,72,96]. Biochemical experiments have shown that monomer recruitment increases adoption of the short pitch state compared to WASP alone[70,73,74,94]. This suggests that monomer recruitment has a role in stimulation of the short pitch state, but the existence of an additional required role has been proposed[74]. Mathematical modeling suggests the nucleus cannot be a dimer, meaning that direct monomer tethering may be required to assemble an actin-Arp2-Arp3 nucleus prior to branch elongation[36]. Though the precise role of monomer recruitment in activation is unclear, its requirement in WASP-mediated activation programs additional regulatory mechanisms into the assembly of actin networks. Network density is influenced by competition for a pool of monomers between WASP and elongating barbed ends, with reduced branch nucleation as the number of barbed ends increases[97]. The WH2

domain also binds barbed ends, competing with capping protein, which increases WASP activity by blocking its barbed end binding[98].

Type II NPFs, including cortactin[99], Abp1[100], and Pan1[101], activate the Arp2/3 complex via a distinct mechanism in which they bind to actin filaments instead of monomers[102]. A well characterized type II NPF is cortactin, which contains a N-terminal acidic (NtA) region that binds to Arp3 but fails to stimulate the short pitch conformation[72,103]. Without increased adoption of the short pitch state, cortactin only weakly activates the Arp2/3 complex, but can potently synergize with type I NPFs[104]. An additional role for type II NPFs is that of branch stabilization[100,105]. This is evidenced by observations of cortactin remaining stably bound to branch junctions after nucleation. Furthermore, a structure of the branch junction shows cortactin bound to Arp3 and the daughter filament, stabilizing the active conformation and Arp2/3-actin contacts[104,106]. Though type II NPFs have multiple functions, further characterizations are needed to determine their primary role in functional actin networks.

During WASP-mediated activation, the Arp2/3 complex must bind to the side of an existing actin filament to nucleate a branch. The ARPC2 and ARPC4 subunits form the majority of contacts at the filament interface, with additional interactions made by Arp3, ARPC1, and ARPC3[78,80 77,79]. Though the filament binds at the clamp, adoption of the short pitch state does not substantially change the contacts made with the filament in the inactive state, suggesting that filament binding does not influence clamp twisting during stimulation of the short pitch state[78]. Biochemical crosslinking assays have also shown that filaments do not stimulate the short pitch state, instead influencing a distinct conformational change[107]. Structural evidence suggests this is flattening as Arp3 flattening increases contacts with the mother filament through movement of Arp3 and ARPC3[78]. This requirement to bind a preformed actin filament ensures that WASP-

mediated activation creates a branch rather than a linear filament, allowing assembly of highly dendritic actin networks. Because of this binding requirement in activation, Arp2/3 complex must navigate vast, dense networks consisting of many potential binding sites and may need to tune its binding affinity to avoid sequestration and localize to WASP at the membrane.

Arp2/3 complex nucleates linear filaments when activated by the WISH/DIP/SPIN90 (WDS) family of proteins[45]. WDS proteins contain armadillo repeat motif (ARM) domains, through which they bind to ARPC2 and ARPC4 in the Arp2/3 complex[81,108]. Because this binding site does not clash with the D-loops of incoming monomers as in the WASP-mediated mechanism, WDS proteins can remain bound to the Arp2/3 complex after nucleation resulting in a "single turnover" event, balancing relative levels of branched and linear actin[109]. Structural evidence shows that the same conformational changes occur in Arp2/3 complex during linear filament nucleation as in branch nucleation, with subtle differences[76,78]. Biochemical experiments investigating the role of the *S. pombe* WDS protein Dip1 in activation found that Dip1 stimulated the short pitch conformation at levels similar to WASP[45]. That the WDS-mediated mechanism of linear filament nucleation does not require filament binding suggests that WDS proteins also stimulate flattening of Arp2/3 complex. Though WDS proteins can activate Arp2/3 complex without a type I NPF, they also synergize with WASP family proteins to nucleate linear filaments[110]. The WDS mediated mechanism of linear filament nucleation plays important roles in network assembly and architecture. The linear filament nucleation activity of Arp2/3 complex may provide seed filaments required for the assembly of branched actin networks. Because branch nucleation requires a pre-existing filament, there must be a source of seed filaments driving network formation. Additionally, recent structures have demonstrated that the mammalian WDS protein SPIN90 acts as a dimer with biochemical

experiments showing that its activity is dependent on its dimerization domain[111,112]. How the nucleation of bidirectional filaments influences network architecture and functionality remains to be seen.

In my dissertation, I seek to elucidate the regulatory mechanisms involved in activation of the Arp2/3 complex and their influence on functionality of polarized networks. In Chapter II, I investigate the role of actin monomer recruitment in branch nucleation. In Chapter III, I investigate the influence of perturbations of the equilibrium between the splayed and short pitch states on functional actin networks. In Chapter IV, I investigate the role of binding affinity for filaments in Arp2/3 complex activation.

CHAPTER TWO

DIRECT ACTIN MONOMER DELIVERY IS A WASP-SPECIFIC REQUIREMENT FOR HUMAN ARP2/3 COMPLEX ACTIVATION

*This chapter contains previously published co-authored material.

Carlson S. and Nolen B. Direct actin monomer delivery is a WASP-specific requirement for human Arp2/3 complex activation. Journal of Molecular Biology. (under revision). (2025).

Author Contributions: Sofia Carlson and Brad Nolen conceptualized the study, designed experiments, and wrote and edited the manuscript. Sofia Carlson generated reagents and performed experiments.

Introduction

Polymerizing actin filaments play critical roles in cellular force production. New actin filaments are formed when the first few actin subunits (or structural mimics of actin) associate to create the filament nucleus, the smallest oligomer that elongates at its ends at the same rate as actin filaments[113]. Filament nucleation is tightly regulated to control when and where actin networks assemble and to dictate their cellular architectures[46], both of which are critical for defining cytoskeletal function. While several actin filament nucleators have been identified, including Arp2/3 complex, formins, and tandem WH2 proteins, Arp2/3 complex is the only nucleator known to nucleate branched actin filaments[44,114,115]. Branched actin networks assembled by Arp2/3 complex drive many biological processes, including endocytosis, cellular motility, autophagy, and tissue morphogenesis[1–4,6]. Precise control of the nucleation activity of Arp2/3 complex is essential to properly orchestrate these processes.

While Arp2/3 complex is intrinsically inactive, several classes of activating proteins, or Nucleation Promoting Factors (NPFs), trigger its activation. The largest class of NPFs—the Type I or WASP-family NPFs— includes several members, including WASP, N-WASP, WAVE, WHAMM, JMY, WHIMP, and WASH[3]. WASP family proteins are characterized by the presence of a C-terminal WCA (or VCA) segment (WH2, Central, Acidic), which constitutes the minimal region sufficient for activation[85,116]. The CA sequence within WCA binds Arp2/3 complex at two distinct sites, and engagement at both sites is required for maximal activation[74,92,117,118]. The WH2 sequence binds to actin monomers, allowing WASP to deliver the first actin subunits for incorporation into the new filament[85,119]. WASP constructs lacking the WH2 region activate Arp2/3 complex weakly or not at all, demonstrating that recruitment of actin monomers is critical for nucleation during WASP-mediated activation[85,116]. Importantly, the requirement for directly recruited monomers establishes competitive interactions that regulate both branch density and WASP activity in Arp2/3-assembled actin networks. First, by creating competition between WASP and actin filament barbed ends for the pool of unpolymerized monomers, this requirement limits the number of branches that can be nucleated, thereby controlling branch density within the networks[97]. Second, actin binding by the WH2 domain establishes competition between WASP and capping protein for filament barbed ends, allowing capping protein to indirectly stimulate WASP by preventing its association with barbed ends[98]. Despite these essential regulatory roles, how WASP-recruited actin monomers contribute to activation is still unclear.

Arp2/3 complex must bind to WASP, WASP-recruited actin monomers, and the side of a pre-existing actin filament before nucleation is triggered[85,86]. Activation involves two major structural changes: movement of the Arp2 and Arp3 subunits into an arrangement that matches

consecutive actin subunits along the short pitch helical axis of the actin filament (the short pitch conformation), and subunit flattening in both Arp2 and Arp3[74,78,81,120]. These changes allow the Arp2-Arp3 pair to structurally mimic a filamentous actin dimer and template assembly of the new filament. Biochemical experiments demonstrated that WASP-recruited actin monomers stimulate movement of Arp2/3 complex into the short pitch conformation, thus bringing the complex closer to a nucleation-competent state, indicating that this may be their primary contribution to activation[73,74,94,120]. However, when researchers crosslinked an engineered human Arp2/3 complex to lock it into the short pitch state, it remained inactive and still required WASP for activation[74]. This finding suggested that in addition to stimulating the short pitch state, actin monomers delivered during WASP-mediated activation play a second essential role in triggering nucleation.

While the nature of this additional role is unclear, one model proposes that direct actin monomer recruitment is a fundamental requirement to build the actin filament nucleus during activation by any NPF. Several lines of evidence support this model. For instance, kinetic modeling showed that the filament nucleus during spontaneous actin assembly is at least a trimer or tetramer of actin[113,121], suggesting the Arp2-Arp3 filament-like dimer may be insufficient to constitute a nucleus. Additionally, studies of tandem WH2 class of actin filament nucleators indicated that direct tethering and self-association of actin monomers via WH2 segments is a viable mechanism to complete nucleus construction[44,115,122]. However, some data argue against the requirement for direct monomer delivery during Arp2/3 complex-mediated nucleation. For instance, in budding yeast Arp2/3 complex (ScArp2/3 complex), WASP must directly deliver actin monomers for potent activation under normal conditions, but when the complex is crosslinked into the short pitch conformation, ScArp2/3 complex nucleates actin filaments

potently even without WASP-recruited actin monomers[120]. These data indicate that direct actin monomer delivery is not a fundamental requirement for nucleation by ScArp2/3 complex, but rather a specific requirement for WASP-mediated activation.

These apparent discrepancies may reflect fundamental mechanistic differences between Arp2/3 complexes from distinct species. Biochemical and structural investigations have used purified human, bovine, budding yeast, fission yeast, and *Acanthamoeba* Arp2/3 complex. These experiments—in addition to the crosslinking data mentioned above—have revealed multiple differences among the distinct species. For instance, while Arp2/3 complexes from both yeast and mammals retain some nucleation activity in the absence of NPFs, this basal activity is greater in the budding yeast complex[123], likely due to its increased propensity to populate the short pitch conformation[74,120]. Furthermore, mammalian but not yeast Arp2/3 complexes are regulated through phosphorylation of the Arp2 subunit[124,125]. While these species-specific differences could be symptomatic of fundamental differences in the nucleation mechanism, it is also possible that they represent minor evolutionary adaptations, and that the overall mechanism of nucleation is conserved. Here we use a combination of biochemical assays and kinetic modeling to distinguish between these possibilities, and to address the role of actin monomer delivery in nucleation by human Arp2/3 complex. Our data clarify how actin filament nuclei can be assembled by Arp2/3 complex during activation of the complex by any NPF, with or without monomer delivery, and demonstrate that fundamental aspects of the nucleation mechanism are conserved between yeast and mammalian complexes.

Results

Short pitch crosslinked HsArp2/3 complex may be inactivatable

To better understand how recruited actin monomers influence the activity of human Arp2/3 complex (HsArp2/3 complex), we revisited the short pitch crosslinking assays of Zimmet, et al[74]. Their data showed that treating dual cysteine engineered HsArp2/3 complex with bismaleimidoethane (BMOE) yielded mixed products. These included ~20% crosslinked complexes, as well as an unknown percentage of uncrosslinked complexes and BMOE adducts. The BMOE-treated reaction mix was not active without WASP and was only partially activated by WASP. This led to the conclusion that the crosslinked HsArp2/3 complex was inactive without WASP, but activatable by WASP, whereas the non-crosslinked BMOE adducts were not fully activatable. An alternative interpretation is that the human complex is inactive upon crosslinking, possibly locked into a near, but not fully short-pitch state. To assess this possibility, we engineered the previously studied cysteines that trap the short pitch conformation (between residues Arp3 (L117C) and Arp2 (L199C)) into HsArp2/3 complex containing high-activity subunit isoforms (Arp3A, ARPC1B, and ARPC5L). We purified this complex using an insect cell expression system with His-Strep tags on ARPC1 (Figure 2.1A). The purification procedure yielded low milligram quantities of Arp2/3 complex that showed consistent activity across preparations (Figure S2.1A).

HsArp2/3-dual cysteine (wildtype HsArp2/3 from here onward) was active in the presence of the VCA fragment of N-WASP in pyrene polymerization assays but showed little or no activity in the absence of N-WASP VCA, consistent with previous reports (Figure S2.1A). We treated the human dual cysteine complex with the bismaleimide crosslinker BMOE and found an optimized condition in which up to 40% of the complex was crosslinked after

incubation with BMOE in the absence of N-WASP (Figure 2.1B). These data are consistent with the previous report and suggest that the HsArp2/3 complex at least weakly adopts the short pitch conformation even in the absence of WASP[74]. To determine how crosslinking affects Arp2/3 complex activity, we tested the products of the reaction—a mix of uncrosslinked and crosslinked complexes— in pyrene actin polymerization assays. These assays showed that neither the crosslinked nor the uncrosslinked adducts have significant activity in the absence of N-WASP-VCA, consistent with previous data[74] (Figure 2.1C and 2.1D). To determine whether HsArp2/3 complexes in the crosslinked mix are activatable, we added N-WASP-VCA to the pyrene polymerization assays. We found the crosslinked mix had reduced WASP-stimulated activity compared to the untreated HsArp2/3 complex (Figure 2.1E). From these data, we cannot rule out

Figure 2.1. Short pitch crosslinked HsArp2/3 complex may be inactivatable.
(A) Coomassie-stained SDS-PAGE gel of purified human dual-cysteine Arp2/3 complex containing tandem 12x His and TwinStrep tags on the ARPC1 C-terminus. (B) (left) Anti-Arp3 western blot of 0.5 μM dual-cysteine HsArp2/3 complex crosslinked for 1 hour with 25 μM BMOE. (right) Quantification of percent Arp2/3 crosslinked (n=3). (C) Time course of pyrene actin polymerization comparing the activity of the uncrosslinked versus crosslinked human Arp2/3 complexes in the absence of N-WASP-VCA. Reactions contained 3 μM 15% pyrene labeled actin and the indicated concentrations of crosslinked or uncrosslinked Arp2/3 complex. The control reaction contained 15 nM uncrosslinked complex and 50 nM N-WASP-VCA. (D) Maximum polymerization rates calculated from reactions in (C). Statistical significance was determined by an ordinary one-way ANOVA with Dunnett's multiple comparisons test (n=4). (E) Time course of pyrene actin polymerization comparing the activity of the crosslinked reaction mixture (total Arp2/3 concentration 25 nM) with 50 nM added N-WASP-VCA to the indicated concentrations of the purified uncrosslinked Arp2/3 complex with the same concentration of N-WASP-VCA. Reactions contained 3 μM 15% pyrene labeled actin. (F) Maximum polymerization rates calculated from reactions in (E). (n=4) (G) Possible percent activities of the crosslinked Arp2/3 complex (magenta) and uncrosslinked Arp2/3 complex (green) that could produce the activity of the complex measured in (E). The activity of the BMOE-treated reaction mix, which contains a total of 9.6 nM crosslinked and 15.4 nM uncrosslinked Arp2/3 complex (which likely includes BMOE adducts), has activity equivalent to ~11 nM non-BMOE treated complex. This activity could be accounted for by the inactive crosslinked Arp2/3 complex harboring no activity and the uncrosslinked pool being 71% active (left extreme in plot), the crosslinking complex being 100% active and the uncrosslinked pool having 9% activity (right extreme in plot), or by the intermediate scenarios indicated in the plot.

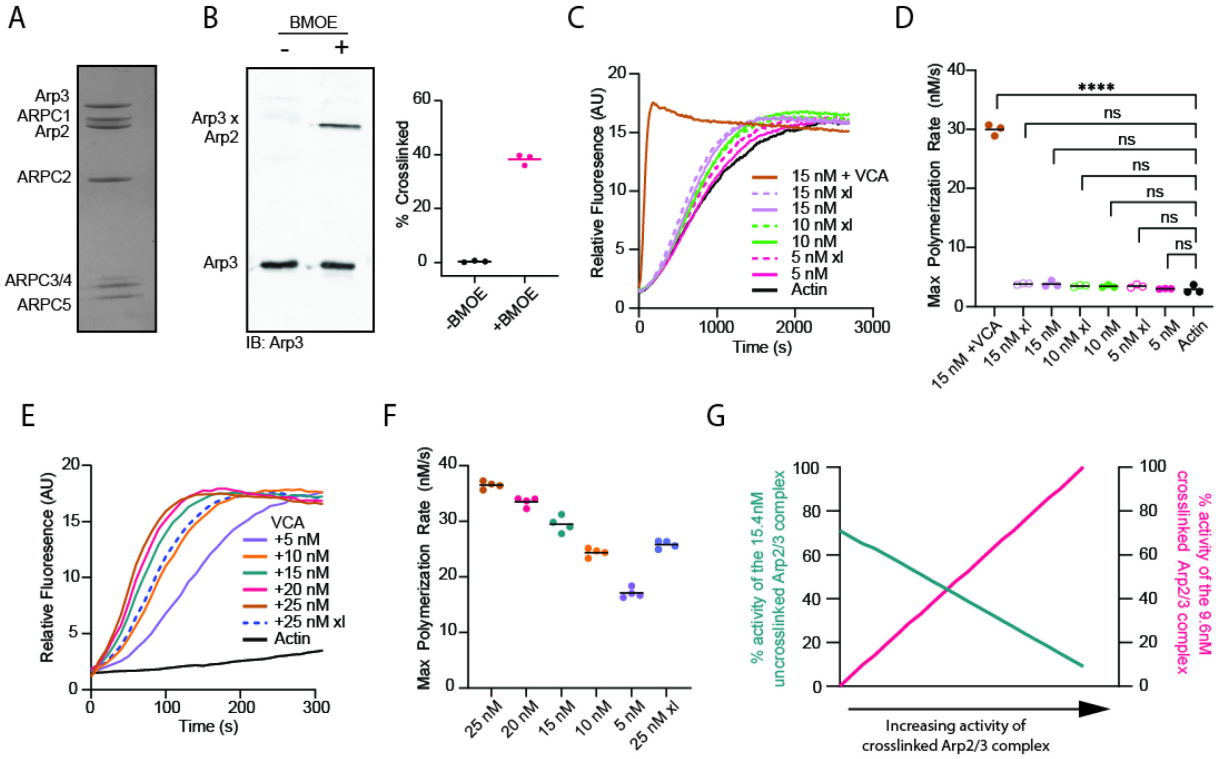

the possibility that uncrosslinked BMOE adducts are defective. However, a 25 nM HsArp2/3 complex reaction mix containing 38.4% (9.6 nM) crosslinked and 61.6% (15.4 nM) uncrosslinked had slightly more activity than a reaction containing 10 nM uncrosslinked HsArp2/3 complex (Figure 2.1E and 2.1F). This level of activity can be attributed to either a complete loss of activity in the crosslinked fraction of the reaction mixture or various degrees of partial activity loss in both the crosslinked and uncrosslinked fractions (Figure 2.1G). These results support the possibility that the short pitch crosslinked complex may be inactive, even in the presence of WASP. We conclude that this assay cannot be used to determine whether locking the HsArp2/3 complex into the short pitch conformation bypasses the need for WASP and WASP-recruited actin monomers in the activation mechanism.

Splayed interface mutations stimulate NPF-independent activity in HsArp2/3 complex

We found that activity measurements of the crosslinked mixes were ambiguous, so we switched to a mutagenesis approach to assess the effect of adoption of the short pitch conformation on HsArp2/3 complex activity. In ScArp2/3 complex, mutations at the inactive (splayed) interface between Arp2 and Arp3 destabilize the splayed state, shifting the equilibrium towards the short pitch state[126]. We purified the homologous single point mutants in HsArp2/3 complex, Arp2 (A208W) and Arp2 (F204Y), in the context of the dual engineered cysteines and tested whether they shifted the conformational equilibrium by crosslinking each mutant with BMOE (Figure 2.2A and 2.2B). Crosslinking between the Arp2 and Arp3 subunits increased in both Arp2 (F204Y) and Arp2 (A208W) complexes compared to the wildtype complex, demonstrating that the mutations increase the population of the short pitch conformation (Figure 2.2C and 2.2D). Based on the previously published results[74], we expected that the shift toward the short pitch conformation would not be sufficient to activate the complex without WASP, as fully short pitch crosslinked HsArp2/3 complex was reported to have no WASP-independent activity. However, the splayed interface mutants showed significant activity in the absence of WASP (Figure 2.2E-2.2G). The activity of the Arp2 (F204Y) and Arp2 (A208W) mutants, as measured by the maximum polymerization rate, was 60% and 45% greater than the wild-type complex, respectively, in reactions using 25 nM of the Arp2/3 complexes. The mutant complexes were less active than the wild-type complex activated with an optimal concentration of WASP, consistent with the observation that the mutants only partially shift the complex toward the short pitch conformation (Figure 2.2D). These data demonstrate that activation of the short pitch HsArp2/3 complex does not require direct recruitment of actin monomers by WASP. They also indicate that BMOE crosslinking creates a defective HsArp2/3 complex. Unlike the

splayed interface mutants, the crosslinked complex showed no NPF-independent activity despite being locked in the short pitch conformation, suggesting that crosslinking itself impairs complex function (Figure 2.1C and 2.1D).

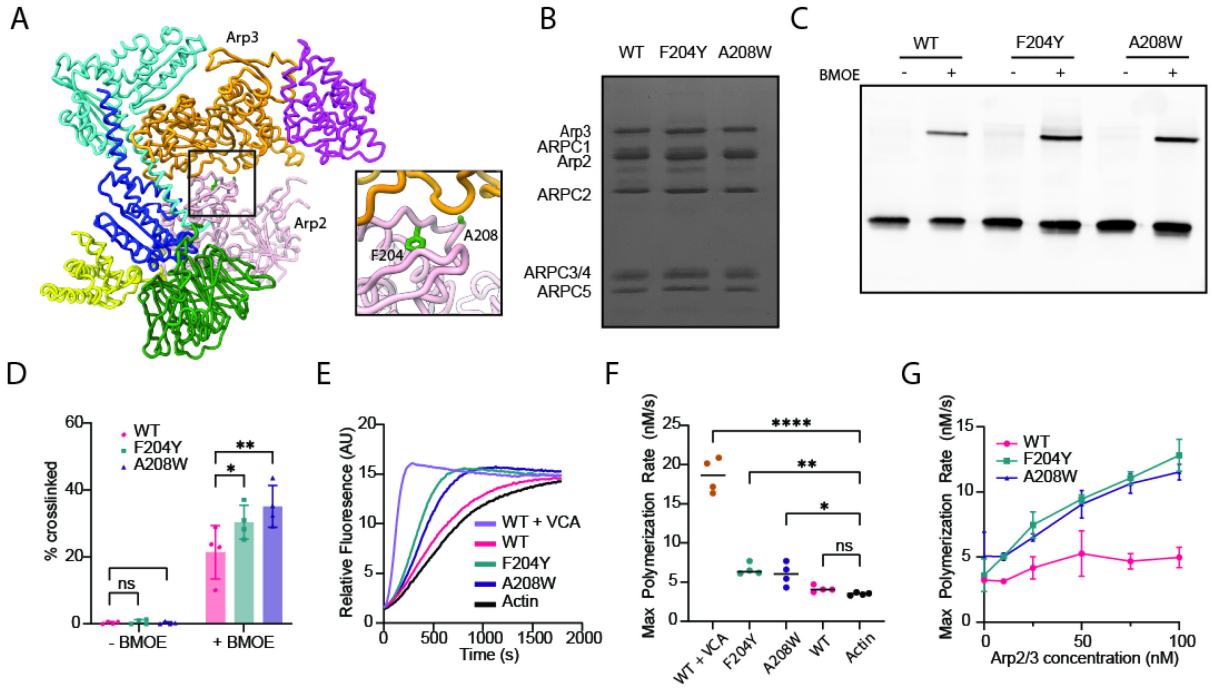

Figure 2.2. Splayed interface mutations stimulate NPF-independent activity in HsArp2/3 complex. (A) Structure of inactive *Bos taurus* Arp2/3 complex highlighting residues in Arp2 at the Arp2-Arp3 splayed interface, A208 and F204 (PDB: 4jd2). These residues are conserved in human Arp2/3 complex and are mutated in this study. (B) Coomassie-stained SDS-PAGE gel of purified human Arp2/3 complexes: wild-type dual-cysteine construct (WT), Arp2(F204Y) and Arp2(A208W). (C) Anti-Arp3 western blot of 0.5 µM WT, Arp2(F204Y), and Arp2(A208W) complexes crosslinked for 30 minutes with 25 µM BMOE. (D) Percent crosslinked WT, Arp2(F204Y), and Arp2(A208W) complexes from reactions in (C). Statistical significance was determined by an ordinary two-way ANOVA with Dunnett's multiple comparisons test (n=4). (E) Time courses of pyrene actin polymerization for reactions containing 3 µM 15% pyrene labeled actin and either 25 nM Arp2(F204Y), Arp2(A208W), or WT complexes in the absence of N-WASP VCA or 25 nM WT Arp2/3 complex with 100 nM N-WASP-VCA. (F) Maximum polymerization rates calculated from reactions in (E). Statistical significance was determined by an ordinary one-way ANOVA with Dunnett's multiple comparisons test (n=4). (G) Plot of maximum polymerization rates versus concentration of Arp2/3 complex for wild-type and mutant complexes under the reaction conditions shown in E. No N-WASP-VCA was present in these reactions. Error bars indicate standard deviation (n=3).

Splayed interface mutants likely require monomer collision for WASP-independent nucleation

Our data demonstrate that direct actin monomer recruitment is not required to activate HsArp2/3 once it adopts the short pitch conformation. This indicates either that the Arp2-Arp3 short pitch dimer alone is sufficient to create the filament nucleus, or that monomers diffuse, collide with and bind to the Arp2-Arp3 dimer to construct the nucleus. To distinguish between these possibilities, we ran time courses of pyrene actin polymerization with varying concentrations of the Arp2(A208W) complex and modeled the reactions using kinetic simulation software. To minimize the number of floating rate constants in the simulations, we first modeled spontaneous actin assembly by running the assays at a range of actin concentrations without Arp2/3 complex (Figure S2.2). The best-fit rate constants for actin dimerization and trimerization were used for Arp2 (A208W) modeling.

We modeled WASP-independent activation of the Arp2(A208W) complex using several different pathways to determine which reaction schemes fit the time courses we measured in the pyrene actin polymerization assays (Figure 2.3A, Table S2.1). Each model included an irreversible branching nucleation step to represent activating conformational changes (e.g., subunit flattening or adoption of the short pitch conformation). This step was made irreversible to prevent subunit dissociation from converting elongating branches into new branch nuclei, since the simulations do not account for filament length[104,127]. While rate constants for actin filament binding by wild-type or mutant HsArp2/3 complexes have not been measured, we floated the off rate and constrained the on rate based on measured binding affinities of HsArp2/3 complex for actin filaments[74,128]. In the simplest model (Arp2-Arp3 dimer nucleus model, Figure 2.3A), Arp2/3 complex bound a preformed actin filament, underwent irreversible activation, and

the Arp2-Arp3 heterodimer formed the nucleus for branch elongation. This model fit the data poorly, suggesting that the Arp2-Arp3 heterodimer alone is insufficient to build the nucleus (Figure 2.3B).

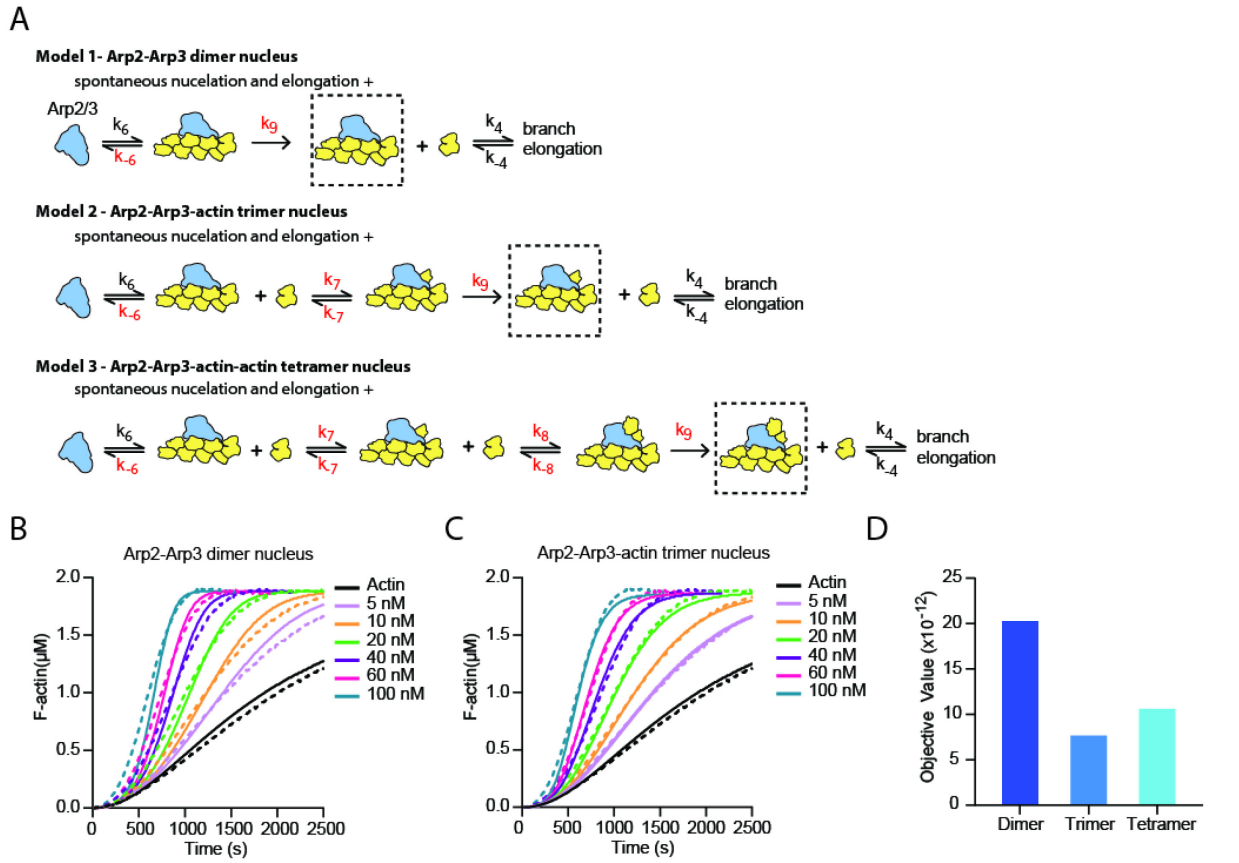

Figure 2.3. Splayed interface mutants likely require monomer collision for WASP-independent nucleation. (A) Pathways of WASP-independent nucleation by the Arp2(A208W) complex mutant tested via mathematical modeling. Each pathway also included reactions for spontaneous nucleation in the simulation (see Figure S2.2). The filament nucleus is indicated by the dashed box in each pathway. Floated rate constants are in red and fixed or constrained rate constants (see main text) are in black. (B) Polymerization time courses (dashed lines) of 15 % 2 μM pyrene labeled actin with the indicated concentrations of Arp2(A208W) Arp2/3 complex. Best fits from Model 1 (Arp2-Arp3 dimer nucleus model) simulations are shown as solid lines. (C) Polymerization time courses as described in (B). Best fits from Model 2 (Arp2-Arp3-actin trimer nucleus model) simulations are shown as solid lines. (D) Objective values of the best fits from Model 1-3. Objective value is the result of minimization of the normalized weighted sum of squares (see methods).

The poor fits in the Arp2-Arp3 dimer nucleus model show that accumulation of polymer is faster than predicted by the simulation early in the reaction and slower later in the reaction. We wondered whether this could reflect dependence on the actin monomer concentration, which decreases as the reaction proceeds. Therefore, we next considered a model in which an actin monomer must collide with the complex and bind to Arp2 and Arp3 to form the nucleus (Arp2-Arp3-actin trimer nucleus model, Figure 2.3A). This model fit the data well, suggesting that monomers must collide with and bind to Arp2/3 complex for activation (Figure 2.3C). We also tested a model requiring two actin monomers to bind the complex, but these simulations fit poorly compared to those in the Arp2-Arp3-actin trimer nucleus model (Figure 2.3D). Together, these data suggest the Arp2-Arp3 heterodimer is insufficient for nucleation, and that a monomer must collide with and bind to the complex to create the nucleus. We note that the WASP-independent activity of the Arp2(F204Y) complex also fit best to the Arp2-Arp3-actin trimer nucleus model, indicating the splayed interface mutants use similar NPF-independent nucleation mechanisms (Figure S2.3, Table S2.2).

SPIN90 achieves potent Arp2/3 activation through monomer collisions

Our data indicate that direct actin monomer delivery is not required to activate HsArp2/3 complex once it is shifted into the short pitch state. However, our simulations suggest that actin monomers must bind to the complex to build the branch nucleus. While random collisions allow an actin monomer to bind to the complex in the best fitting model (Arp3-Arp2-actin trimer nucleus model), we expect this step to be comparatively slow, since direct monomer delivery by WASP dramatically increases the effective concentration of actin monomers. Therefore, we wondered whether nucleus formation through (slow) monomer collisions could yield rapid

nucleation by mammalian Arp2/3 complex, or if directly tethered monomers are required for rapid nucleation. We could not address this with the splayed interface mutants, as these mutants had relatively weak WASP-independent activity that could be attributable either to their incomplete adoption of the short pitch conformation and/or because of slow actin monomer collision steps. Instead, we compared the nucleation potency of SPIN90, the mammalian WISH/DIP1/SPIN90 (WDS) protein, to N-WASP, a prototypical WASP family protein.

Like other WDS proteins, SPIN90 activates BtArp2/3 complex without directly delivering monomers[45], so we reasoned that the SPIN90-Arp2/3 complex might build a filament nucleus through one or more monomer collisions. To test this, we measured activation of the complex by a range of concentrations of SPIN90 and modeled the resulting pyrene actin polymerization time courses using multiple kinetic pathways (Figure 2.4A, Table S2.3), as described above. While it is now known that dimerization is required for SPIN90 activity, for simplicity we did not include SPIN90 dimerization steps in the models[111,112]. In the simplest activation pathway, SPIN90 bound reversibly to Arp2/3 complex followed by an irreversible activation step, with the Arp2-Arp3 heterodimer creating the nucleus (SPIN90 Arp2-Arp3 dimer nucleus model). As with the splayed interface mutants, this model fit the data poorly (Figure 2.4B), suggesting the Arp2-Arp3 heterodimer is insufficient to create the nucleus. A model in which a single actin monomer collided and bound to SPIN90-Arp2/3 complex to create the nucleus showed an improved fit (SPIN90 Arp2-Arp3-actin trimer nucleus model, Figure 2.4A) (Figure 2.4C), and a model requiring two monomers fit similarly to the single monomer-binding pathway (Figure 2.4D). These observations suggest SPIN90-mediated activation, like the NPF-independent activity of the splayed interface mutants, requires assembly of an Arp2-Arp3-actin nucleus with at least one actin monomer.

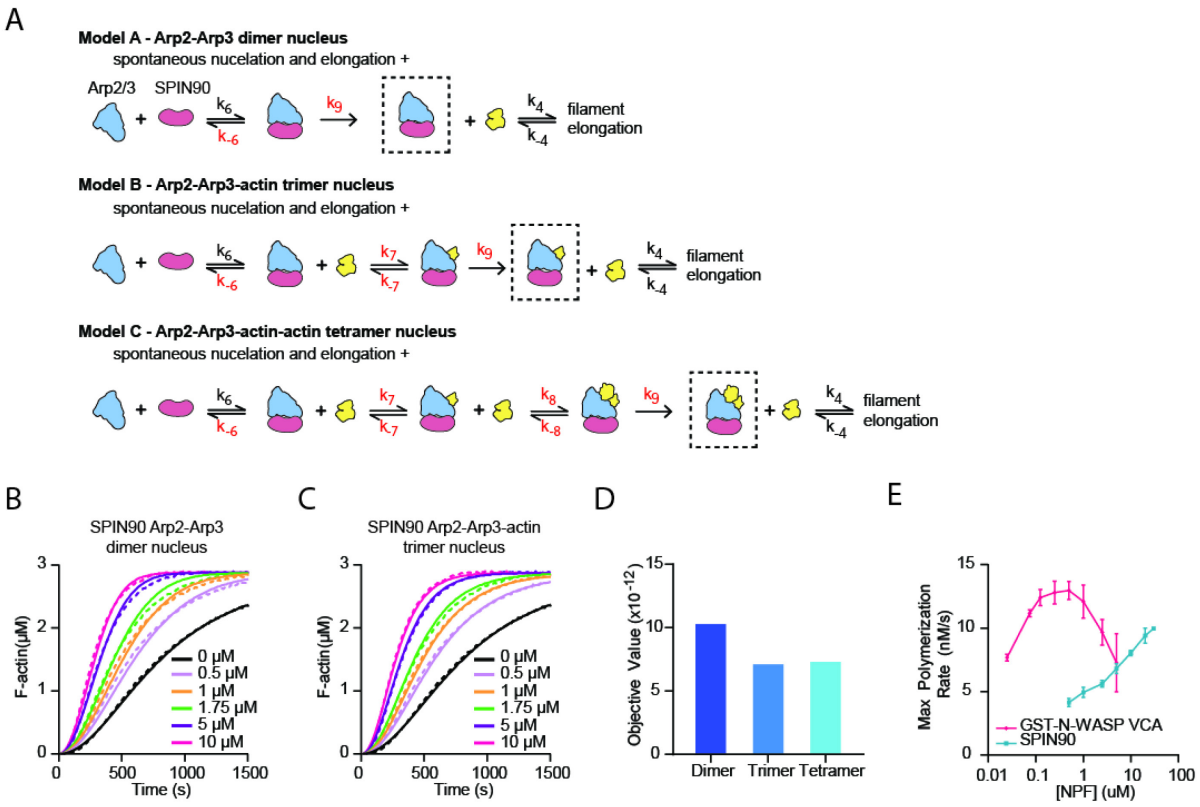

Figure 2.4. SPIN90 achieves potent Arp2/3 activation through monomer collisions
(A) Pathways of SPIN90-mediated activation of HsArp2/3 complex tested via mathematical modeling. The filament nucleus is indicated by the dashed box in each pathway. Floated rate constants are in red and fixed or constrained rate constants (see main text) are in black.
(B) Polymerization time courses (dashed lines) of 15 % 3 μM pyrene labeled actin with 25 nM *Bos taurus* (Bt)Arp2/3 complex and the indicated concentrations of SPIN90. Best fits from Model 1 (SPIN90 Arp2-Arp3 dimer nucleus model) simulations are shown as solid lines.
(C) Polymerization time courses as show in (B) with best fits from Model B (SPIN90 Arp2-Arp3-actin trimer nucleus model) simulations shown as solid lines. (D) Objective values of the best fits from dimer (Figure 2.4B), trimer (Figure 2.4C), and tetramer models. Objective value is the result of minimization of the normalized weighted sum of squares (see methods).
(E) Plot of maximum polymerization rates versus concentration of either SPIN90 or GST-N-WASP-VCA [NPF] for pyrene polymerization assays containing either NPF plus 3 μM 15% pyrene labeled actin and 25 nM BtArp2/3 complex. Error bars indicate standard deviation (n=3).

To determine whether SPIN90-mediated activation can yield rapid nucleation despite relying on random monomer collisions, we directly compared the activity of SPIN90 and N-WASP-VCA in pyrene actin polymerization time courses (Figure 2.4E). More SPIN90 was required to saturate Arp2/3 complex than N-WASP-VCA, suggesting that it binds Arp2/3 complex weakly. However, at near-saturating concentrations, SPIN90 stimulated nucleation by the complex at levels close to that triggered by N-WASP-VCA, according to their maximum polymerization rates. This suggests that—even though it relies on collision and binding of untethered monomers—SPIN90 can stimulate relatively rapid filament nucleation in bulk polymerization assays.

To better understand the rates of the monomer binding and nucleation steps in the SPIN90 reaction, we examined the fittted kinetic rate constants for k_{-7}, k_7 and k_9, but found that they were poorly determined by the data (Figure S2.4C-E). Therefore, we derived an equation to express the macroscopic rate constant for formation of new ends from the SPIN90-Arp2/3 complex assembly ($k_{obs,\ S90}$) (Figure S2.4A-B). This rate constant describes the rate through the monomer collision and nucleation steps during SPIN90-medidated activation. Because of the simple, linear pathway of the model, the value for $k_{obs,\ S90}$ is well-determined at ~0.0001 s^{-1} Figure S2.4C-E.

Because of the non-linear nature of the mechanism, we could not derive an analogous macroscopic rate constant for monomer binding and nucleation steps during WASP-mediated activation, as modeled in Helgeson, et al (reactions 23, 24, and 25 in Figure S2.5A)[129]. Therefore, to estimate the rates of these steps, we used previous measurements of the binding kinetics of actin to an isolated WH2 domain along with the nucleation rate constant derived from single molecule studies of the budding yeast Arp2/3 complex[85,130]. Given these values, we

estimated a $k_{obs,WASP}$ of ~0.0067 s^{-1} for the WASP monomer binding and nucleation steps at 3 μM actin monomer (Figure S2.5B). This value is ~70 fold faster than the analogous macroscopic rate constant for the SPIN90 mechanism. While not definitive, these calculations are consistent with a model in which actin monomer collisions and subsequent nucleation steps during SPIN90-mediated activation are slower than WASP-mediated actin monomer recruitment, at least at 3 uM actin.

Discussion

Our data demonstrate that direct actin monomer delivery is a WASP-specific requirement, not a fundamental prerequisite for Arp2/3 activation. Why direct monomer delivery is required for WASP but not WDS family proteins may relate to their distinct binding modes and release requirements. WASP proteins must be released before nucleation completes because their binding is incompatible with the final nucleation-competent conformation[74,78,93,104]. In contrast, WDS proteins remain bound throughout activation and even after nucleation is complete[109]. Therefore, direct monomer delivery by WASP may be required to stimulate release of WASP from the nascent branch junction. Consistent with this hypothesis, engagement of the D-loops of recruited actin monomers with the barbed end grooves of Arp2 and Arp3 is thought to cause activating structural changes (e.g. subunit flattening) that could facilitate WASP release[81]. These interactions could explain why monomer delivery is needed during WASP-mediated activation and, while not required, how it can accelerate activation by other NPFs (see below).

We show here that—comparing near-saturating NPF concentrations of each NPF—SPIN90 activates *Bos taurus* (Bt)Arp2/3 complex at rates similar to N-WASP-VCA, despite its inability to recruit actin monomers. A similar comparison revealed that the *S. pombe* WDS

protein, Dip1, activated Arp2/3 complex more potently than *S. pombe* WASP at all concentrations tested, even though Dip1 relies on monomer collisions rather than delivery[45]. Together, these findings demonstrate that collision-based nucleation mechanisms can result in significant activation of the complex relative to WASP, despite the slow passage through the monomer binding and nucleation steps. Simulations of the WASP-mediated activation pathway suggest that despite relatively rapidly monomer binding and nucleation steps, WASP-mediated nucleation may be at least partially limited by slow actin filament binding in these assays (Figure S2.6). In contrast, SPIN90 does not require preformed filaments for activation, so its rate of new filament end creation is similar to WASP despite its slower passage through the monomer binding and nucleation steps. Therefore, the kinetics of SPIN90-mediated activation are consistent with its role in initiating rather than propagating branched actin networks: it has high activity relative to WASP at low filament concentrations and low activity relative to WASP at high actin filament concentrations.

Importantly, WDS proteins activate more potently when monomer delivery is incorporated into the reaction. Specifically, both Dip1 and SPIN90 potently synergize with WASP proteins to activate Arp2/3 complex[110,131]. This synergy depends on the ability of WASP to deliver actin monomers to the complex, suggesting that WASP-mediated monomer delivery eliminates the slow monomer collision step to accelerate nucleation. This principle may extend to cortactin, a weak type II NPF that lacks monomer binding regions and likely depends on collisions for nucleation[99,132]. Fusing WASP's actin-binding region to cortactin dramatically enhances its potency[133]. Understanding why monomer delivery or collisions are required—and why the Arp2-Arp3 dimer alone is insufficient—remains an important open question in understanding the Arp2/3 complex nucleation mechanism.

Our findings indicate that fundamental aspects of activation are conserved between yeast and mammalian Arp2/3 complexes. Specifically, both mammalian and yeast complexes can be activated without the need to directly recruit actin monomers once they adopt the short pitch conformation (e.g., by WDS proteins or through splayed interface mutations). In contrast, during activation by WASP, both yeast and human complexes require direct actin monomer recruitment through the WASP WH2 domain, a requirement essential for regulating WASP activity and branch density in Arp2/3-assembled branched actin networks[97,98].

The conserved roles of actin monomers in activating human and yeast complexes, despite ~1.5 billion years of evolutionary divergence, suggests that other fundamental aspects of the activation may also be preserved. However, it will be important to test other key aspects of the mechanism to confirm this hypothesis. For instance, actin filaments play a well-understood role in WASP-mediated activation of ScArp2/3 complex, where crosslinking experiments showed that actin filaments do not stimulate the short pitch conformation but instead stimulate a different conformational change[107]. Whether this is also true for mammalian complexes will be critical to test, given that the filament requirement ensures that only branched actin filaments are nucleated during WASP-mediated activation.

While crosslinked ScArp2/3 complex gains potent NPF-independent activity[120], our data indicate that the crosslinked HsArp2/3 complex is defective and cannot be activated. The structural basis for this difference is unclear, but comparison of the active BtArp2/3 complex structure (*Bos taurus* Arp2 and Arp3 show 100% identity to their human homologues) to a ScArp2/3 complex homology model revealed potentially important differences near the crosslinked cysteines[78]. For instance, within 5 Å of the two crosslinking residues are three substitutions that may create more steric crowding around the BMOE crosslinker in HsArp2/3

complex: Arp3 Hs T119 (Sc P157), Arp3 Hs H192 (Sc N230), and Arp2 Hs L198 (Sc S197) (Figure S2.7). Molecular dynamics simulations indicate that BMOE has an S-S crosslinking distance of ~6.3-10.5 Å, depending on its conformation[134]. We speculate that steric crowding may force BMOE in crosslinked HsArp2/3 complex to adopt a conformation that holds Arp2 and Arp3 in a non-native inactive state. Additional computational and structural work will be required to test this hypothesis and to understand the conformational diversity of the nucleation-competent ensemble.

Methods

Cloning, protein expression, and purification

Actin was purified from rabbit muscle acetone powder and labeled with pyrene iodoacetamide as previously described[110]. N-WASP-VCA (C431A) and GST-N-WASP-VCA were purified as previously described[120]. Human SPIN90 (269-722) was purified as previously described[108], with minor changes as follows. Protein was eluted from the Resource 30Q column over a salt gradient from 50 to 400 mM NaCl. After passing through a glutathione Sepharose column, protein was purified on a Superdex 75 column, followed by a Superdex 200 column, pooling pure fractions each time. Pure protein was concentrated in a Vivaspin Turbo 30 concentrator (Sartorius) and exchanged into storage buffer (20mM Tris pH 8.0, 100mM NaCl, 1mM DTT) before flash freezing in liquid nitrogen and storing. *Bos taurus* Arp2/3 complex was purified as previously described from calf thymus[135]. Proteins described above are shown in Figure S2.1B.

Human Arp2/3 complex was expressed using the biGBac insect expression system[136]. The Arp3A, ARPC1B, and ARPC5L isoforms were used as complexes with these variants have

been shown to be more active than their counterparts[137]. C-terminal tandem 12x His and TwinStrep tags were added to the ARPC1 subunit. Arp2, Arp3, ARPC1, ARPC2, ARPC3, ARPC4, ARPC5, and a mNeonGreen (mNG) fluorescent marker were subcloned into pLIB vectors with polyhedrin promoters. The dual-cysteine mutant was constructed by introducing mutations Arp2 (L199C), Arp3 (L117C), and Arp3 (C408A) into pLIB Arp2 or pLIB Arp3 via site directed mutagenesis. The dual-cysteine construct used in the crosslinking activity assays (Figure 2.1) had the additional mutations C189A and C307A introduced by site-directed mutagenesis into pLIB Arp3. F204Y and A208W mutations were introduced into the Arp2 pLIB vector via site-directed mutagenesis in the context of the dual-cysteine mutation. Genes from pLIB vectors were then PCR amplified and inserted via Gibson or Infusion (Takara) assembly into linearized parent pBIG1 vectors to produce three pBIG1 vectors containing Arp2 and Arp3, ARPC1-3, or ARPC4-5 and mNG. pBIG1 vectors were then digested with the PmeI restriction enzyme and inserted via Gibson assembly or Infusion into a linearized parent pBIG2 vector to produce a single pBIG2 vector containing all seven subunits and the mNG fluorescent marker to track viral infection.

Bacmid DNA was generated by transforming pBIG2 plasmids into DH10Bac competent cells and purifying with GeneJET Plasmid Miniprep kit (ThermoFisher) through the neutralization step with subsequent purification by ethanol precipitation. Sf9 cells maintained in ESF921 media (Expression Systems) with 2% fetal bovine serum (FBS) were transfected with purified Bacmids by incubating 5-7 µg of DNA with 4 µL of FuGENE (Promega) and 250 µL of Opti-MEM media (Gibco) for 20 minutes before adding to 1 x 10^6 cells in a 6-well plate. After 4-7 days at 27° C, the supernatant (P0 virus) was added to 7 x 10^6 Sf9 cells in a 10 cm tissue culture dish, which were grown for another 4-7 days at 27°C. These cells were harvested by

centrifugation at 600 x g for 5-10 minutes and the supernatant (P1 virus) was stored at -80 °C. P2 virus was prepared by infecting 100 mL of Sf9 cells at 1 x 10^6 with 2 mL of P1 virus and harvesting after 4-7 days by centrifugation at 600 x g for 5-10 min, filtering with a 0.22 µm polyethersulfone (PES) filter, and storing at 4° C. Protein was expressed in HighFive cells maintained in ESF921 media by infecting with 2% P2 virus at log phase and growing for 2 days. Cells were harvested via centrifugation after addition of 1mM EDTA and 1mM phenylmethylsulfonyl fluoride (PMSF). Cell pellets were washed with phosphate-buffered saline (PBS), pelleted via centrifugation, and stored at -80 °C until purification.

Arp2/3 complex was purified by resuspending cell pellets in PKME buffer (25mM PIPES-KOH pH 7, 50 mM KCl, 1 mM EGTA, 3 mM $MgCl_2$, 1 mM dithiothreitol (DTT), 0.1mM ATP) supplemented with cOmplete Mini EDTA-free Protease Inhibitor Cocktail (Roche) and 1.25 U/mL Benzonase Nuclease (Millipore Sigma) and lysing via sonication. Cell lysate was supplemented with 2 mM PMSF and clarified via ultracentrifugation in a Ti70 or Ti45 rotor for one hour at 52k or 35k RPM. The fat layer was aspirated off and the clarified lysate was filtered once through 8 ply cheese cloth and subsequently through a 5 µm PVDF filter and an optional 0.45 µm PVDF filter. The filtrate was then loaded on a glutathione Sepharose 4B (Cytiva) GST-N-WASP VCA column prepared as previously described[90], washed with PKME, PKME + 25mM KCl, and PKME + 50mM KCl, and then eluted via a 100 mM to 1M NaCl gradient in 20 mM Tris-HCl pH 8, 1 mM BME, and 5% glycerol. The elution was diluted to 250 mM NaCl and 0.5 mM BME and loaded on a HisPur Cobalt Superflow Agarose (Thermo Scientific) and/or nickel–nitrilotriacetic acid (Ni–NTA) affinity column in 20 mM Tris pH 8, 250 mM NaCl, 5 mM imidazole, 0.5 mM BME, and 5 % glycerol before washing with 20 mM Tris pH 8, 250 mM NaCl, 15 mM imidazole, 0.5 mM BME, and 5% glycerol. The cobalt column was eluted with 20

mM Tris pH 8, 250 mM NaCl, 150 mM imidazole, 0.5 mM BME, and 5 % glycerol. The Ni-NTA affinity column was eluted with 20mM Tris pH 8, 250 mM NaCl, 250 mM imidazole, 0.5 mM BME, and 5 % glycerol. Eluted fractions were pooled, supplemented with 1 mM EDTA, 1 mM DTT, and 0.1 % Tween 20, and dialyzed against 20 mM Tris pH 8, 100 mM NaCl, 1 mM DTT, 1 mM EDTA, 0.1% Tween20, and 5% glycerol for 4 hours. The sample was then dialyzed in 20 mM Tris with 100 mM NaCl overnight and then for an additional 4 hours with fresh buffer. The sample was then run over a glutathione Sepharose 4B column to remove any residual GST-N-WASP-VCA before it was concentrated in a stirred ultrafiltration cell (Amicon) with a Hydrosart 30 kDa molecular weight cutoff filter (Sartorius), flash frozen, and stored at -80 °C. Concentrations were determined by measuring absorbance at 280 nm (ε_{280}= 237,000 $M^{-1}cm^{-1}$) and validated via sodium dodecyl sulfate polyacrylamide gel electrophoresis (SDS PAGE). While we were previously able to purify crosslinked budding yeast Arp2/3 complex[107], we did not attempt to purify the crosslinked HsArp2/3 complex because the yields were too low.

Crosslinking assays

Dual-cysteine Arp2/3 complex was incubated in 1x KMEI (10 mM Imidazole-HCl pH 7.0, 50 mM KCl, 1 mM EGTA, 1 mM $MgCl_2$) and 0.2 mM ATP for 5 minutes at room temperature before adding a 50x molar excess of bismaleimidoethane (BMOE). Reactions were carried out at room temperature and quenched with 2 x SDS buffer for western blot or 1 mM DTT for pyrene polymerization assays. For western blot analysis, reactions were run on 10-20% SDS-PAGE gradient gels, transferred overnight onto nitrocellulose membranes, probed with 1:200 Anti-Arp3(A-1) (Santa Cruz sc-48344) primary antibody followed by 1:5000-1:15,000 IRDye 800CW Donkey anti-Mouse IgG secondary antibody (Licor #925-32212)

before imaging on an Amersham Typhoon imager. Quantification of the percent crosslinked was completed in the ImageQuant analysis software by determining the crosslinked and uncrosslinked band intensities after background subtraction via the rolling ball method.

Pyrene actin polymerization assays

Pyrene actin polymerization assays were carried out in a 96-well black flat bottom half-area plate (Corning 3686) on a TECAN Safire 2 plate reader with excitation at 365 nm and emission at 407 nm. A 10x solution of M/E buffer (5 mM $MgCl_2$, 20 mM EGTA) was added to rabbit skeletal muscle actin in G buffer (5 mM Tris pH 8.0, 0.2 mM $CaCl_2$, 0.2 mM ATP, 0.2 mM DTT) with 5% bovine serum albumin (BSA) and the solution was incubated for 2 min. Activators including Arp2/3 complex and indicated proteins were pre-mixed and added to the actin at the concentrations indicated, with a final concentration of 2-3 μM 15% pyrene-labeled actin, and a final buffer composition of 10 mM Imidazole-HCl pH 7.0, 50 mM KCl, 1 mM EGTA, 1 mM $MgCl_2$, 0.2 mM ATP, and 1mM DTT. For mathematical modeling experiments, measurements were made in a cuvette using an ISS PC1 Photon counting spectrofluorometer and BSA was not added to the reaction. Maximum polymerization rates were determined by measuring slopes across 5 time points and converting to elongation rates by assuming that 0.1 μM actin remained unpolymerized at steady state.

Mathematical Modeling

Time courses of actin assembly were simulated using the program COmplex PAthway Simulator (COPASI)[138]. Fluorescent values from actin polymerization assays containing 2 or 3 μM 15% pyrene-labeled actin were converted to the concentration of polymerized actin based on

the assumption that the critical concentration of 0.1 μM actin remained monomeric at steady state. Models were fit with reaction traces for both F-actin and G-actin concentrations for each reaction condition. All conditions were fit simultaneously to each model, first using the genetic algorithm with 800 iterations, followed by the Levenberg-Marquardt method with 2000 iterations for local refinement. Quality of fits were evaluated based on the objective value, determined by calculating the normalized mean square weighted sum of squares (MSS) with the following equation: $MSS = \sum \frac{1}{<x^2>} * (x - y)^2$, with x representing an experimental data point and y the corresponding simulated value.

To reduce the number of floating parameters, reactions containing only actin were fit to spontaneous nucleation and assembly models to determine rate constants for dimerization, trimerization, and trimer nucleation (Figure S2.2). Barbed and pointed end elongation rates were fixed according to previously measured values[35]. The best-fit values were subsequently used when testing models for reactions containing SPIN90, the Arp2(A208W) complex, or the Arp2(F204Y) complex. Actin trimer nucleation values were floated in A208W and F204Y models to account for variation in actin activity between days. Simulations of the polymerization reaction without actin were repeated for each preparation of actin. To constrain Arp2/3 complex filament binding rate constants for A208W and F204Y mutant complex modeling, the K_D was estimated by averaging the estimated K_D from two previous studies on HsArp2/3[74,128]. To constrain SPIN90 binding to Arp2/3 complex, maximum polymerization rates from pyrene polymerization traces over a range of SPIN90 concentrations were plotted. An apparent binding affinity was estimated from the resulting curve with the nonlinear regression curve fit in GraphPad Prism and using the 95% confidence interval range of affinity values. SPIN90 was

recently found to dimerize and nucleate bidirectionally[111,112], but we treated it as a monomer to simplify the model and reduce the number of floating variables.

Rate of barbed end formation was determined for SPIN90 and GST-VCA by plotting the rate of Arp2/3 complex ends versus time in Copasi with the indicated saturating concentration of each activator. The simulations were run with the reported best fit values from model B for SPIN90 and from Table 1 in Helgeson et al for WASP [129].

.

Derivation of k_{obs}

The macroscopic rate constant $k_{obs,SPIN90}$ defines the rate of barbed end formation at steady state from a SPIN90-Arp2/3 complex. The equation used to calculate $k_{obs,SPIN90}$ was derived using the nucleation pathway and values shown in Figure S2.4, assuming a constant concentration of actin monomers.

The macroscopic rate constant $k_{obs,WASP}$ defines the rate of barbed end formation at steady state from a WASP-filament-Arp2/3 complex. The equation used to calculate $k_{obs,WASP}$ was derived using the nucleation pathway and values shown in Figure S2.5, assuming a constant concentration of actin monomers. Because of the non-linear pathway to nucleus formation, we ignored the parallel pathways and included only reactions 23-25 in our derivation. Because we could not use the best fit rate constant values from Copasi, we used previously reported values for WH2 domain actin binding[85,138]: $k_{on} = 4.3 \times 10^7\ M^{-1}s^{-1}$ for k_{23} and k_{24} and $k_{off} = 25.8\ s^{-1}$ for k_{-23} and k_{-24} [85]. For the k_{25} nucleation rate constant, we used a previously reported nucleation rate of $0.007\ s^{-1}$ from budding yeast[130], assuming this rate was equal to that of the bovine Arp2/3 complex.

Structural analysis of crosslink sites

Structural analysis of residues near the crosslink site was completed by comparing the active BtArp2/3 complex structure (PDB:7tpt) to a ScArp2/3 complex homology model created by using the BtArp2/3 complex structure as a template.

Bridge to Chapter III

In chapter II, we showed that activation of the human Arp2/3 complex can occur without monomer recruitment by WASP. Nucleus formation occurs through monomer collisions in activation of Arp2/3 complex mutants that more readily adopt the short pitch conformation and during SPIN90-mediated activation. Bypassing the requirement for monomer recruitment has also been observed in budding yeast, signifying that fundamental aspects of Arp2/3 complex activation are conserved between yeast and humans. These findings clarify how Arp2/3 complex is activated and provide insight into potential requirements for actin nucleation by other nucleators. In Chapter III, I investigate the relevance of these findings *in vivo* by characterizing the effects of splayed interface mutations in Arp2/3 complex during endocytosis in *Saccharomyces cerevisiae***.** Though monomer recruitment is not required for activation of the mutants *in vitro*, the requirement for WASP restricts Arp2/3 complex branch nucleation to the membrane. I seek to determine how disruption of the regulatory splayed to short pitch switch influences the functional actin networks involved in endocytosis.

CHAPTER THREE

CONSTITUTIVELY ACTIVATED ARP2/3 COMPLEX MINIMALLY ALTERS ENDOCYTIC ACTIN ASSEMBLY

*This chapter contains unpublished co-authored material.

Author Contributions: Brad Nolen, Heidy Narvaez-Ortiz, and Sofia Carlson conceptualized the study. Heidy Narvaez-Ortiz and Brad Nolen designed experiments. Heidy Narvaez-Ortiz generated reagents and performed experiments. Sofia Carlson performed data analysis. Sofia Carlson and Brad Nolen wrote and edited the manuscript.

Introduction

The dynamics of many cellular processes such as motility, morphogenesis, and endocytosis require precise regulation[1–6]. This is achieved by machinery consisting of polymerizing actin filaments that form extensive branched networks capable of producing force. To respond to diverse stimuli, actin filaments must assemble into complex architectures at the right place and time. The critical step in the assembly of branched actin networks is the nucleation of each branch, carried out by Arp2/3 complex.

The Arp2/3 complex requires a nucleation promoting factor (NPF) such as a member of the WASP family of proteins, a preformed actin filament, and WASP-recruited monomers for activation[85,86]. During activation, it adopts a short pitch, flattened state, mimicking a filamentous actin dimer. Intra-subunit flattening occurs in the Arp2 and Arp3 subunits, as each transitions out of the actin monomer-like twisted state[33]. Rearrangement into the short pitch state involves a large rigid body movement of half of the Arp2/3 complex, reorienting Arp2 relative to Arp3, moving the Arps into an active conformation that mimics the arrangement of two consecutive

actin subunits along the short pitch axis of an actin filament[78,81]. Biochemical work investigating the role of activators in Arp2/3 complex activation has established that WASP and WASP-recruited actin monomers stimulate the short pitch state[73,74,94,120]. This requirement for the membrane-tethered WASP in Arp2/3 complex activation ensures branch nucleation is restricted to the membrane[88].

Perturbing the splayed to short pitch equilibrium by increasing adoption of the short pitch through crosslinking or point mutations bypasses the requirement for WASP in activation, conferring NPF independent activity[120]. Activity in the absence of WASP is detrimental for functionality of reconstituted force-producing actin networks because nucleation is no longer spatially restricted, leading to unproductive filament nucleation away from the actin network and depleting free actin monomers[107]. The functionality of cellular actin networks may similarly depend on a precise equilibrium between the splayed and short pitch states. In cells, unproductive nucleation can disrupt network architectures that are critical for proper functionality of complex processes. There may be additional regulatory mechanisms in place, however, that can counteract the effects of perturbations in the splayed to short pitch conformational switch. Investigating how critical the splayed to short pitch conformational switch is for proper regulation of cellular actin networks is important for understanding how Arp2/3 complex activation is tied to biological functionality.

Endocytosis is a process that allows for the internalization of cargoes containing extracellular materials, and is important for nutrient uptake and cellular signaling[139]. Though other pathways of internalization occur, the most characterized pathway is clathrin-mediated endocytosis, which occurs in all eukaryotes[139] . A complete endocytic event involves over 50 proteins and proceeds through initiation, recruitment, membrane bending, scission, and

uncoating stages[139,140]. Polymerizing actin filaments provide the force necessary for membrane bending during invagination and the presence of actin networks is required for successful invagination in yeast[141]. Arp2/3 complex and NPFs such as N-WASP in mammals or Las17 in budding yeast localize to endocytic sites[1,142]. Endocytosis stalls upon inhibition of Arp2/3 complex, consistent with an important role for branch nucleation in endocytic force production[25,27].

Endocytosis has been well characterized in budding yeast where endocytic sites form at cortical patches[1]. Through expression of fluorescently tagged endocytic proteins, endocytic patches can be tracked and quantified to obtain insight on the functionality of the actin network[62]. This system can serve to determine how perturbations in Arp2/3 complex influence functional actin networks. By utilizing a previously developed quantification pipeline[118], we investigated how perturbing the splayed to short pitch conformational switch in Arp2/3 complex influences actin assembly during endocytosis. Here we show that mutations that destabilize the splayed interface and confer NPF independent activity *in vitro* alter the dynamics of actin assembly without disrupting the overall functionality of the actin networks involved in endocytosis.

Results

Cells expressing Arp2/3 complex splayed interface mutations do not show ectopic actin networks or gross defects in endocytic actin patches

To investigate the influence of constitutively active Arp2/3 complex on assembly of polarized networks, we constructed *Saccharomyces cerevisiae* strains containing mutations in Arp2 previously characterized *in vitro*. Arp2 (F203Y) and Arp2 (A207C) are at the splayed

interface between Arp2 and Arp3 and have been shown to increase adoption of the short pitch state. This bypasses the requirement for Las17, the WASP protein in budding yeast, breaking the splayed to short pitch regulatory switch, and giving Arp2/3 complex NPF independent activity[126]. The strains also expressed Las17 containing N-terminally tagged mNeonGreen (mNG-Las17) and filament binding protein Abp1 C-terminally tagged with TagRFP-T (Abp1-TagRFP-T) to monitor NPF and actin dynamics during endocytosis. Based on the significant NPF independent activity in polymerization assays *in vitro*, we hypothesized that branch nucleation would occur away from the membrane to the detriment of the force-producing network, resulting in failure to successfully internalize endocytic patches. Surprisingly, there were no obvious defects in the endocytic patches in mutant strains compared to the wildtype strain (Figure 3.1). In all strains, no ectopic actin was observed and Abp1 localized into discrete puncta that were circular and cortical.

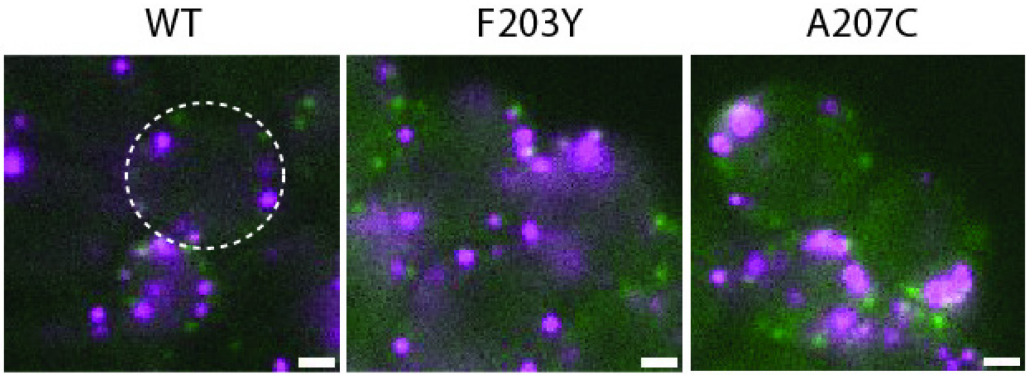

Figure 3.1. Splayed interface mutants do not show ectopic actin networks or catastrophic defects during endocytosis. A) Representative images of wildtype and mutant *Saccharomyces cerevisiae* strains expressing Abp1-TagRFP-T and mNG-Las17 imaged at 25 °C. Dashed circle indicates outline of a single cell. Scale bar represents 1 µm. B) Maximum distance Abp1-TagRFP-T traveled from origin for wildtype and mutant strains. Dashed line at 0.25 µM is the threshold for successful internalization. Percentages above the plot represent the overall success rate for each strain. Each data point represents a single punctum. Statistical significance was determined by an ordinary one-way ANOVA with Dunnett's multiple comparisons test. Error bars represent standard deviation.

Splayed interface mutants influence assembly of endocytic actin networks

Because we did not observe significant defects of actin in the mutant strains, we sought to determine whether the dynamics of actin assembly and disassembly were affected. To monitor dynamics, we analyzed Abp1-TagRPF-T fluorescent signals. In wild type cells, Las17 accumulates at the membrane first, followed by the recruitment of Abp1, which increases to a peak intensity. Internalization then begins during which the Abp1 patch moves inward and actin begins to disassemble, corresponding to a decrease in Abp1 fluorescence. We found that Abp1 puncta had longer lifetimes in Arp2 (F203Y) and Arp2 (A207C) compared to the puncta in the wildtype strain (Figure 3.2A). The number of Abp1 molecules was quantified by calibrating the peak fluorescent signal in the wildtype strain to the previously reported average maximum number of molecules per patch[143]. We found that the maximum number of Abp1 molecules increased in both mutant strains (Figure 3.2C and 3.2D). This suggests that the mutant Arp2/3 complexes may be assembling defective actin networks that are less efficient at force production, as it takes more filamentous actin to internalize patches.

To determine if the mutations in the complex influenced the dynamics of Las17 we monitored the fluorescent signal of mNG-Las17. Mutations did not alter the lifetimes of Las17 patches (Figure 3.2B) but changed the average number of Las17 molecules recruited to endocytic sites, calculated as described for Abp1. Approximately 27 more molecules of Las17 were recruited in the Arp2 (A207C) strain. Previous data suggested Las17 is removed from the plasma membrane by treadmilling endocytic actin networks, creating a negative feedback loop that contributes to network disassembly[144]. A suboptimal actin network may not create an effective feedback loop, explaining the increased accumulation of Las17 in the Arp2 (A207C) strain.

Unexpectedly, the average maximum number of Las17 molecules decreased in the Arp2 (F203Y) mutant, an observation that we cannot currently explain.

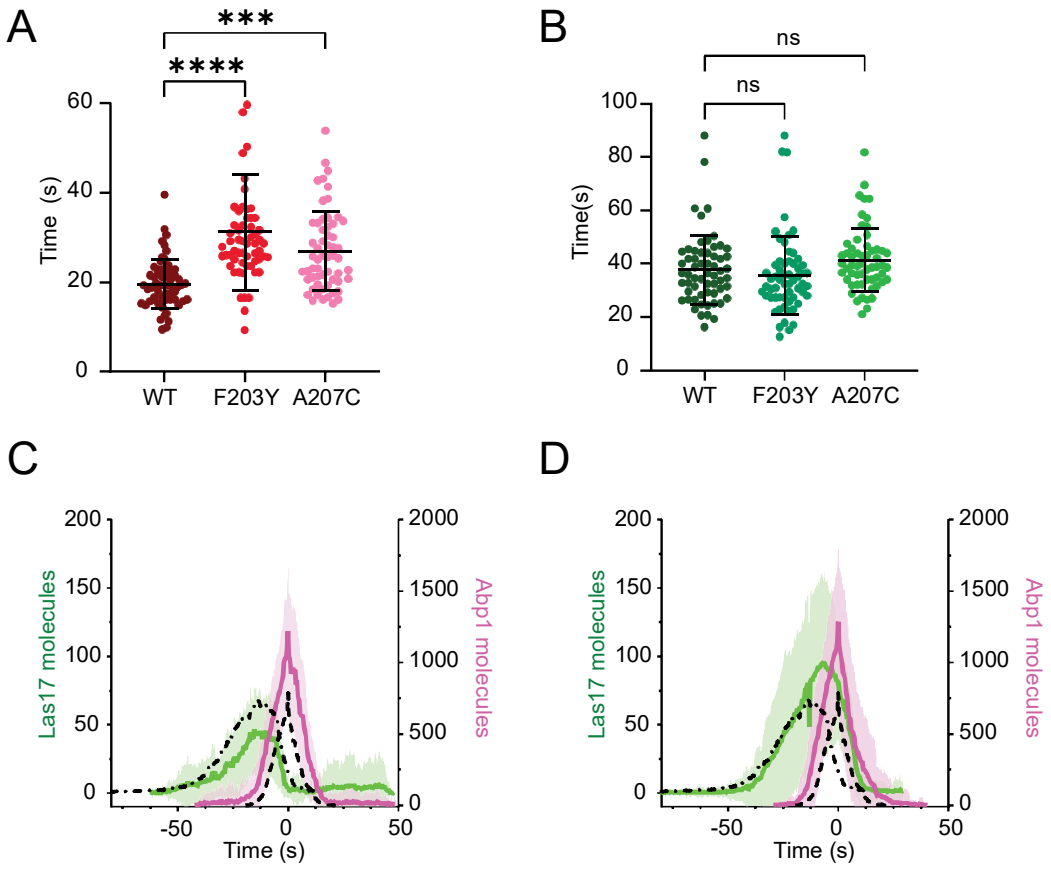

Figure 3.2. Splayed interface mutations alter Abp1 recruitment. A) Plot of Abp1-TagRFP-T lifetimes at endocytic sites for wildtype and mutant strains. Each data point represents a single punctum. Statistical significance was determined by an ordinary one-way ANOVA with Dunnett's multiple comparisons test. Error bars represent standard deviation. B) Plot of mNG-Las17 lifetimes at endocytic sites for wildtype and mutant strains. Each data point represents a single punctum. Statistical significance was determined as described in A. Error bars represent standard deviation. C) Plot of the average number of molecules of mNG-Las17 and Abp1-TagRFP-T over time for the Arp2 (F203Y) (green and magenta) and wildtype (black) strains. Shaded error represents standard deviation. D) Plot of the average number of molecules of mNG-Las17 and Abp1-TagRFP-T over time for the Arp2 (A207C) (green and magenta) and wildtype (black) strains. Shaded error represents standard deviation.

Abp1 accumulation rates are increased in Arp2 (A207C)

Because the Arp2/3 complex splayed interface mutations were previously shown to have increased NPF independent activity in vitro[69], we investigated whether the rate of actin accumulation (as measured by Abp1) at endocytic sites was increased in the mutant strains. We found that the Arp2 (F203Y) mutant accumulated Abp1 at the same rate as the wild-type strain, while the Arp2 (A207C) mutant showed increased accumulation rates of Abp1, suggesting that the mutated complexes have different effects in functional actin networks (Figure 3.3A). This difference perhaps may be attributed to the greater NPF independent activity observed in Arp2 (A207C) *in vitro*[126]. To determine whether disassembly of actin was influenced in the mutant strains, we examined the deaccumulation rates of Abp1, but found no difference compared to wildtype (Figure 3.3B).

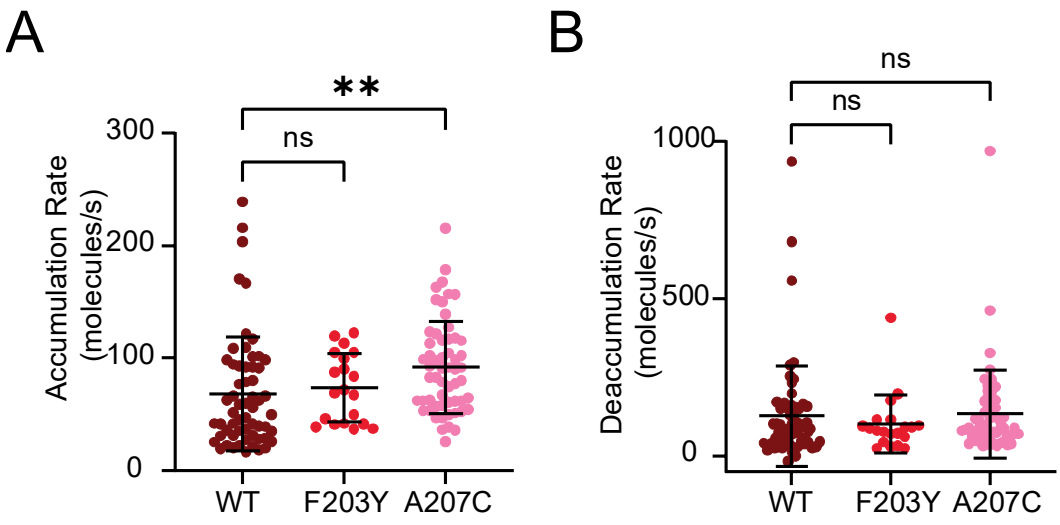

Figure 3.3. Accumulation rate of Abp1-TagRFP-T is increased in Arp2 (A207C) and deaccumulation rate is unchanged. A) Plot of Abp1-TagRFP-T accumulation rates at endocytic sites for wildtype and mutant strains. Each data point represents a single punctum. Statistical significance was determined by an ordinary one-way ANOVA with Dunnett's multiple comparisons test. Error bars represent standard deviation. Error bars represent standard deviation. B) Plot of Abp1-TagRFP-T deaccumulation rates for wildtype and mutant strains. Each data point represents a single punctum. Statistical significance was determined as described in A. Error bars represent standard deviation.

Constitutively active Arp2/3 complex mutants do not show defects in endocytic internalization

To determine if the changed actin and NPF dynamics influenced the functionality of assembled actin networks in endocytosis, we determined whether there were differences in the ability to carry out endocytosis. Successful internalization was defined as an Abp1-TagRFP-T puncta traveling greater than 0.25 µm from its initial location at the membrane. Success rates were similar across all strains indicating that actin networks in mutant strains were still functional, despite changes in their actin assembly dynamics (Figure 3.4).

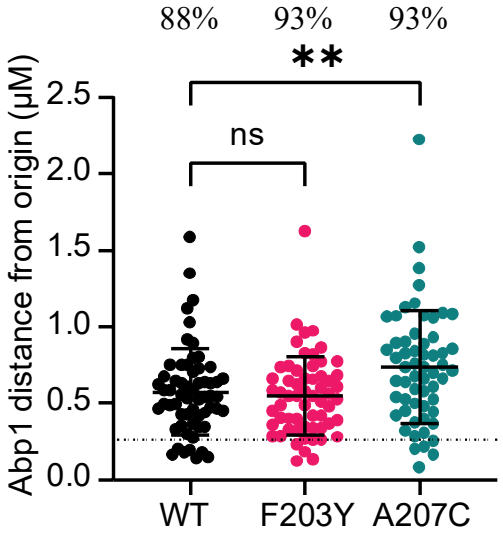

Figure 3.4. Splayed interface mutants do not show defects in endocytic internalization. Maximum distance Abp1-TagRFP-T traveled from origin for wildtype and mutant strains. Dashed line at 0.25 µM is the threshold for successful internalization. Percentages above the plot represent the overall success rate for each strain. Each data point represents a single punctum. Statistical significance was determined by an ordinary one-way ANOVA with Dunnett's multiple comparisons test. Error bars represent standard deviation.

Discussion

Although actin dynamics were altered in cells containing constitutively active Arp2/3 complex, actin networks were still functional. Endocytosis largely proceeded as normal as

determined by the successful internalization of Abp1 patches. This may be a result of additional regulatory mechanisms in place to ensure actin is not assembled unproductively[123]. Out of the 50 proteins involved in endocytosis, some are regulators that may act to inhibit unproductive Arp2/3 nucleation[140]. For example, filament binding proteins such as fimbrin or coronin bind actin filaments to inhibit Arp2/3 complex [145,146], and may prevent unregulated activity within cells. Genetic crosses with strains containing constitutively active Arp2/3 complex and null strains lacking filament binding proteins may clarify the role of other regulators in localized Arp2/3 complex activation.

Another consideration for the relatively minor defects in endocytosis is whether Arp2 (F203Y) and Arp2 (A207C) complexes have similar NPF independent activity in a cellular context compared to *in vitro.* The NPF activity of these mutants was measured with free actin monomers, whereas in cells, actin monomers are predominantly bound to profilin and delivered to Arp2/3 complex by WASP[147,148]. Branching nucleation requires monomer collisions in the absence of WASP-recruited monomers [149]. Profilin-bound actin monomers may be unable to collide with and activate the Arp2/3 complex. If this is the case, the mutant complexes would still require WASP for activation in vivo, thereby preventing unregulated branch nucleation.

Though the actin networks were functional, patch dynamics were altered in the mutant strains, suggestive of defects in actin assembly. Both mutant strains had increased Abp1 accumulation and longer Abp1 lifetimes while Arp2 (A207C) additionally had increased Abp1 accumulation rates. Longer Abp1 lifetimes were similarly observed in constitutively active Arp2/3 complex strains containing multiple mutations in Arp2[150]. Because internalization, Abp1 assembly rates, and total accumulation of Abp1 were not quantified, however, the influence of the mutations on actin assembly dynamics and the success of endocytic internalization were

unknown. The longer lifetimes of actin patches in our mutant strains and the increase in Abp1 molecule recruitment demonstrate that actin assembly is increased, but not productively, either due to branch nucleation independent of WASP or increased nucleation activity in the presence of WASP. This is further supported by the increase in Las17 accumulation in Arp2 (A207C), which suggests that the negative feedback loop that removes Las17 from the membrane is not as effective in this mutant[144]. We hypothesize that the architecture of the actin networks assembled by constitutively active Arp2/3 complexes are sufficient, though suboptimal, for their role in endocytosis.

Methods

S. cerevisiae strain generation

S. cerevisiae strains ScBN358 and ScBN359 were generated by transforming two PCR-generated cassettes into strains containing the Arp2/3 complex mutation of interest (ScBN317, ScBN319) via lithium acetate transformation to add an N-terminal mNeonGreen tag on Las17 and a C-terminal TagRFP-T tag on Abp1 (Table 3.1)[151,152].

Table 3.1. *S. cerevisiae* strains used in this study

Strain	Protein	Genotype	Reference
ScBN369	wild type complex, mNG-Las17, ABP1-TagRFP-T	MATa, ARP3::URA3, his3, leu2, Δarp3::HIS3, natMX6::mNeonGreen-Las17, ABP1-TagRFP-T::kanMX6	[118]
ScBN317	Arp2 A207C	MATa, Arp2-A207C::URA3, his3Δ200, leu2-3,112, lys2-801(oc)?, ade2-1?, Δarp2::HIS3, ABP1::EGFP_NAT	This study
ScBN319	Arp2 F203Y	MATa, Arp2-F203Y::URA3, his3Δ200, leu2-3,112, lys2-801(oc)?, ade2-1?, Δarp2::HIS3, ABP1::EGFP_NAT	This study
ScBN358	Arp2 A207C, mNG-Las17, ABP1-TagRFP-T	MATa, Arp2-A207C::URA3, his3Δ200, leu2-3,112, lys2-801(oc)?, ade2-1?, Δarp2::HIS3, natMX6::mNeonGreen-Las17, ABP1-TagRFP-T::kanMX6	This study

Table 3.1, continued.

Strain	Protein	Genotype	Reference
ScBN359	Arp2 F203Y, mNG-Las17, ABP1-TagRFP-T	MATa, Arp2-F203Y::URA3, his3Δ200, leu2-3,112, lys2-801(oc)?, ade2-1?, Δarp2::HIS3, natMX6::mNeonGreen-Las17, ABP1-TagRFP-T::kanMX6	This study

S. cerevisiae live-imaging and analysis

S. cerevisiae strains were grown, imaged, processed, and analyzed in triplicate as previously described[78,118] using a DeltaVision Ultra High-Resolution Widefield Fluorescence microscope (Cytiva), a pco.edge 4.2 sCMOS camera, an Olympus 100× 1.4 numerical aperture Oil UPlanSApo objective, and B-G-O-FR polychroics. Each video was 1 minute and 15 seconds long, with 100 ms exposure and 10% transmission in the orange and green channels.

Videos were processed in FIJI for background subtraction photobleaching correction[153], TrackMate[154] patches were manually selected, and a custom python script[118] was run to extract fluorescent trajectories for each patch as previously described[118]. This output data aligned based on the maximum intensity of Abp1, including fluorescent values, distance from origin, and lifetimes. Fluorescence levels were corrected by subtracting the average minimum fluorescence value. These corrected values were then converted to number of molecules by multiplying by the ratio of the average maximum number of molecules in patches previously reported[143] (Abp1: 800 ; Las17: 102) to the average maximum fluorescence value in the wildtype strain. Accumulation rates were calculated from the slope between the first value and the maximum value. Deaccumulation rates were calculated from the slope between the maximum value and the last value. Successful internalization was determined by a distance from origin value greater than 0.25 μm.

Bridge to Chapter IV

In Chapter III, I examined the importance of the regulation of the splayed to short pitch conformational switch during cellular actin assembly by expressing constitutively active splayed interface mutations in yeast. I showed that activating mutations of Arp2/3 complex alter actin assembly, but not to the detriment of endocytosis. The amount of actin accumulated and its lifetime in endocytic patches was increased, but patches were still internalized at success rates similar to wildtype strains. Cells likely have regulatory mechanisms in addition to the splayed to short pitch switch that regulate its activity. In chapter IV, I investigate how intrinsically disordered regions of Arp2/3 complex located at the filament binding interface may influence its activity by regulating its binding. Tuning its binding affinity for actin filaments may be important for proper localization to the membrane to avoid unproductive sequestration.

CHAPTER FOUR

INTRINSICALLY DISORDERD REGIONS AT FILAMENT BINDING INTERFACE ARE REQUIRED FOR OPTIMAL HUMAN ARP2/3 COMPLEX ACTIVATION

*This chapter contains unpublished co-authored material.

Author Contributions: Sofia Carlson and Brad Nolen conceptualized the study, designed experiments, and wrote and edited the manuscript. Sofia Carlson generated reagents and performed experiments.

Introduction

Branched actin networks produce force for cellular processes such as cell migration, endocytosis, and cell division by building dense arrays of polymerizing actin filaments at membranes[1–5]. Numerous proteins regulate branched actin networks through the spatiotemporal coordination of assembly, remodeling, and turnover. Critical to the assembly of actin networks is the nucleation of each branch, carried out by the Arp2/3 complex. The Arp2/3 complex nucleates branched filaments upon activation by a nucleation promoting factor (NPF), predominantly the WASP family of proteins, actin monomers recruited by WASP, and an actin filament[85,86]. WASP is membrane-tethered, ensuring branch nucleation is restricted to the region adjacent to the membrane, effectively creating an active zone of nucleation and producing a polarized actin network[95]. After an actin network is initiated, the Arp2/3 complex must typically diffuse through a dense actin network to reach membrane-bound WASP for activation. This localization is important to sustain the network amidst the rapid turnover that occurs in dynamic structures such as the lamellipodial protrusions involved in cellular motility[155]. These networks can be vast; lamellipodium are wide (10-40 μm) structures with high actin density[17]. Because Arp2/3

complex binds actin filaments as part of its activation mechanism, it must avoid sequestration through unproductive binding of actin filaments away from the membrane.

The Arp2/3 complex may avoid unproductive sequestration through its binding interface with actin filaments. Previous work examining the filament binding step of Arp2/3 complex activation found that complexes from different species bind relatively weakly to actin filaments, with K_D values in the low micromolar range[74,127,128,130]. Additionally, filament binding has been observed to be at least partially rate limiting during nucleation[130]. This contrasts with its tight binding at the branch junction where it remains bound after nucleating a branch. Branches are quite stable in the absence of disassembly factors, persisting for minutes *in vitro*[156]. This conservation of weak binding despite tighter binding being favorable for nucleation suggests weak filament binding may be important to rapidly target Arp2/3 complex to membrane-bound WASP.

Previous work in budding and fission yeast suggests that certain structural features may have evolved to attenuate the affinity of the Arp2/3 complex for actin filaments. The Arp3 D-loop, a flexible segment located at the filament binding interface, is found across diverse species, though its sequence and length is not conserved. Though disordered in structures of inactive or Dip1-bound Arp2/3 complex[53,76,108], it becomes ordered to varying extents upon filament binding. Specifically, structures of the bovine Arp2/3 complex at the branch junction show a fully ordered Arp3 D-loop[82], whereas only a portion is ordered in the branch junction with the *S. pombe* (Sp) Arp2/3 complex[79]. In yeast, deletion of this D-loop increased the affinity for actin filaments 2-fold and increased nucleation activity *in vitro*[68]. This suggests that increased binding affinity for filaments is favorable for assembly of isotropic actin networks in which Arp2/3 complex and WASP diffuse freely. The regulatory role of the Arp3 D-loop may arise in the

assembly of polarized actin networks where decreased affinity for actin filaments may ensure effective targeting to the membrane. Another intrinsically disordered region (IDR), the ARPC2 C-terminus, has not been well characterized but may have a similar role. The C-terminal residues of ARPC2 are located at the branch interface, found ordered in the SpArp2/3 complex branch junction structure but remaining disordered in the bovine structure[77,82]. The location of the ARPC2 C-terminus at the mother filament signifies it may also influence filament binding. The presence of multiple IDRs in the Arp2/3 complex may be important for tuning the binding affinity for actin filaments.

Here we show that deletion of intrinsically disordered regions in the human Arp2/3 complex decreases its nucleation activity, in contrast to what was observed in yeast. Additionally, we introduce the design of potential mutations in the Arp2/3 complex that are predicted to increase its affinity for filaments. Utilization of low and high affinity complexes will facilitate future work investigating how affinity for actin filaments influences the ability of the Arp2/3 complex to localize effectively in polarized networks.

Results

Deletion of conserved intrinsically disordered regions decreases activity of human Arp2/3 complex

To determine how intrinsically disordered regions may influence the activity of human (Hs) Arp2/3 complex, we engineered and purified complexes containing deletions of regions near the filament binding interface whose presence is conserved across diverse species. These included the Arp3 D-loop (38-53) and the ARPC2 C terminus (282-300), which are located at the interface between the Arp2/3 complex and the mother actin filament (Figure 4.1). Constructs

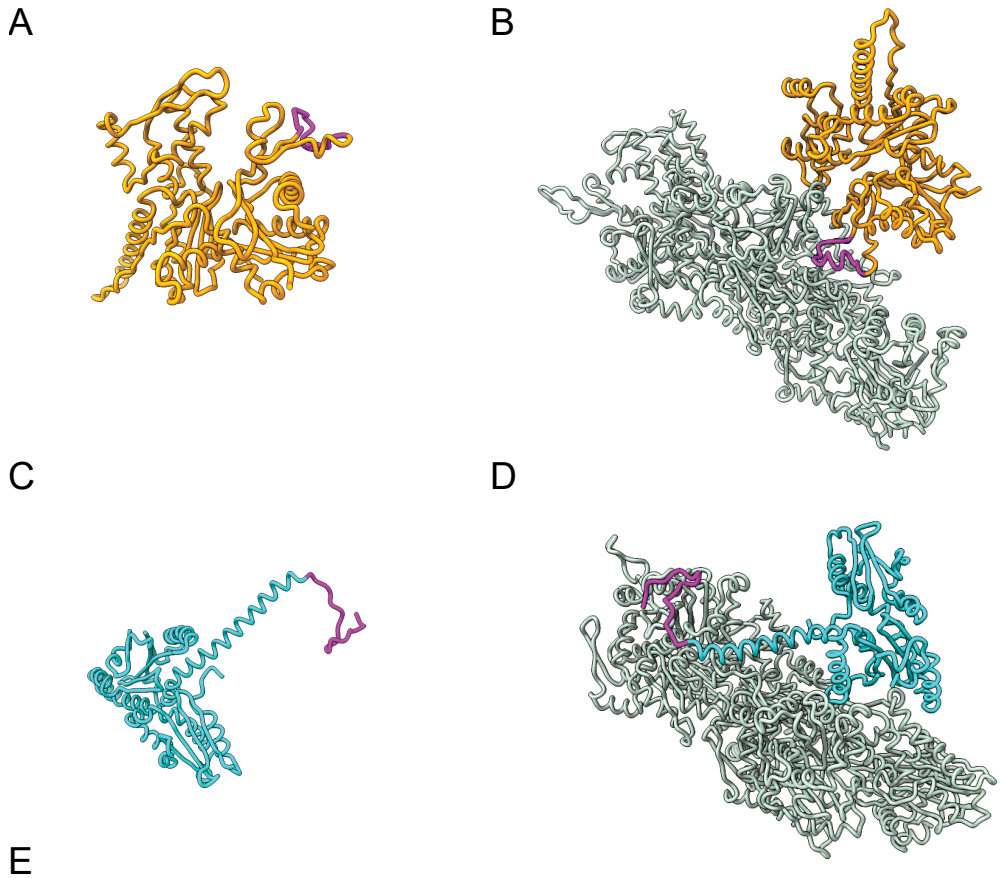

E

```
Hs  38 KESAKVGD----------------------------------QAQRRVMKGV  55
Bt  38 KESAKVGD----------------------------------QAQRRVMKGV  55
Sc  39 AAPSNTKKSSGVGAPSAVSNEASYFGNSTSATNFNGATGGLLSNNLSGKRGT  90
Sp  38 RSAGAS-------SGPAVSSKPSYMAS-------------KGSGHLSSKRAT  69
```

F

```
Hs 274 LKVLNRARPDAEKKEMK-TITGKTFSSR--------- 300
Bt 274 LKVLNRARPDAEKKEMK-TITGKTFSSR--------- 300
Sc 306 IKVLNRAKVDEDDENDELSAEGRQQARRTFTGRKIVY 342
Sp 292 QKVLNRAKPDVELER-K-TATGRSFVRA--------- 317
```

Figure 4.1. Conserved intrinsically disordered regions are located at the filament binding interface. A) Structure of BtArp3 D-loop (PDB: 7tpt). B) Location of BtArp3 D-loop at the mother actin filament interface (PDB: 7tpt). C) Structure of SpARPC2 C-terminus (PDB: 8uxw). D) Structure of SpARPC2 C-terminus at the mother actin filament interface (PDB: 8uxw). E) Sequence alignment of Arp3-D loop. Residues deleted in this study are highlighted in red, residues shown in the structure in A and B are highlighted in magenta, and residues deleted in the previous study[68] are highlighted in blue. F) Sequence alignment of ARPC2 C-terminus. Residues deleted in this study are highlighted in red and residues shown in the structure in C and D are highlighted in magenta.

were purified using an insect cell expression system with tandem 12x His and TwinStrep tags on the ARPC1 C-terminus. The activity of the mutant complexes was determined via pyrene polymerization assays. Unexpectedly, and contrary to what has been seen in *S. cerevisiae* (Sc) Arp2/3 and SpArp2/3 complexes, both ARPC2 ΔC-terminus and Arp3 ΔD-loop complexes had lower activity than the wildtype complex (Figure 4.2). This indicates that these IDRs have a role during activation of the Arp2/3 complex, though not as a "bumper" for filament binding as in yeast.

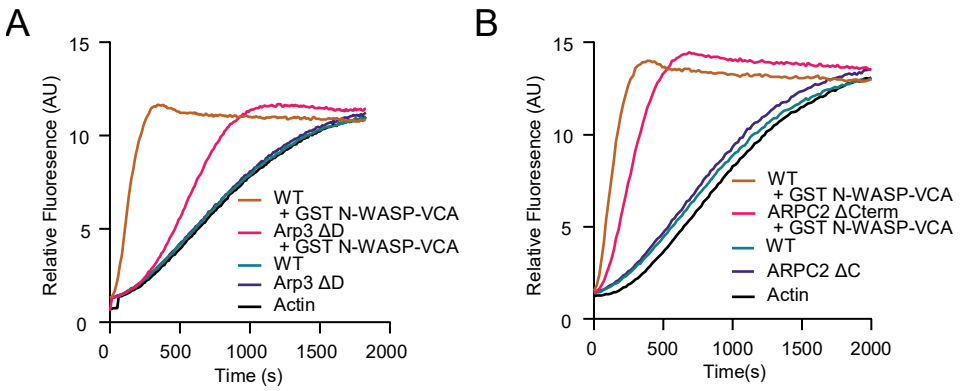

Figure 4.2. Deletion of Arp3 D-loop or ARPC2 C-terminus reduces Arp2/3 complex nucleation activity. Time course of pyrene actin polymerization comparing the activity of 20nM Arp3 ΔD-loop (A) or ARPC2 ΔC-term (B) to wildtype Arp2/3 complex with and without 50nM GST-N-WASP-VCA Reactions contained 3 μM 15% pyrene labeled actin.

Design of a tighter filament binding Arp2/3 complex

To determine whether increased filament binding affinity influences the activity of the HsArp2/3 complex similarly to ScArp2/3 complex, we began engineering an Arp2/3 complex through protein design. Additional characterization of this high-affinity construct in polarized networks will clarify the influence of binding affinity on targeting. We prepared a structure of the inactive HsArp2/3 complex docked on an actin filament and utilized Rosetta to design mutations predicted to improve the filament : complex interface. This Rosetta design protocol

produced ten models, each with dozens of mutations. To evaluate the most probable mutations for a tighter binding construct, we examined the most common mutations in the 10 models (Table 4.1). These included residues at the filament interface, on every subunit except Arp2 and ARPC3, including the ARPC1 protrusion helix and the Arp3 D-loop (Figures 4.3 and 4.4). Further structural analysis, purification, and characterization will be required to determine whether a complex with these mutations has increased affinity as predicted.

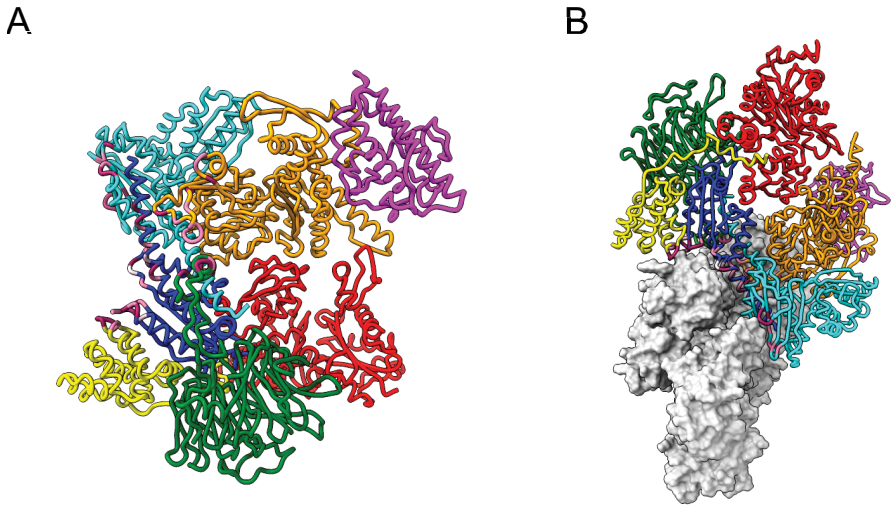

Figure 4.3. Most common mutations predicted by Rosetta to improve filament binding interface. A) Location of mutated residues colored by conservation between models (dark magenta: frequently mutated/less conserved, white: rarely mutated/more conserved). B) Location of predicted mutations at the mother filament interface colored as in A. PDB: 4jd2.

Table 4.1. Most common Rosetta-predicted mutations.
Most common mutations in the 10 Rosetta-designed structures, listed if found in at least 3 of the constructs.

Subunit	**Mutations**
Arp3	E39S, K42P, G44I, D45F, Q46T, V51E, P70Y, T71F, A73E
ARPC1	A298T, R299K, Q303V, L305R, D306A, K307E, S310P
ARPC2	K157S, R160V, S192N, H193P, T194A, P206L, L207E, E208Q, T224L
ARPC4	A3N, T4A, L5F, R6A, Y8F, R55L, E59V, K77I/P/T, D80T, I82Q, E83M, D143L, S147I, K150F/L, N154W, A155Y
ARPC5	D119N, N120D, S122A, A123I

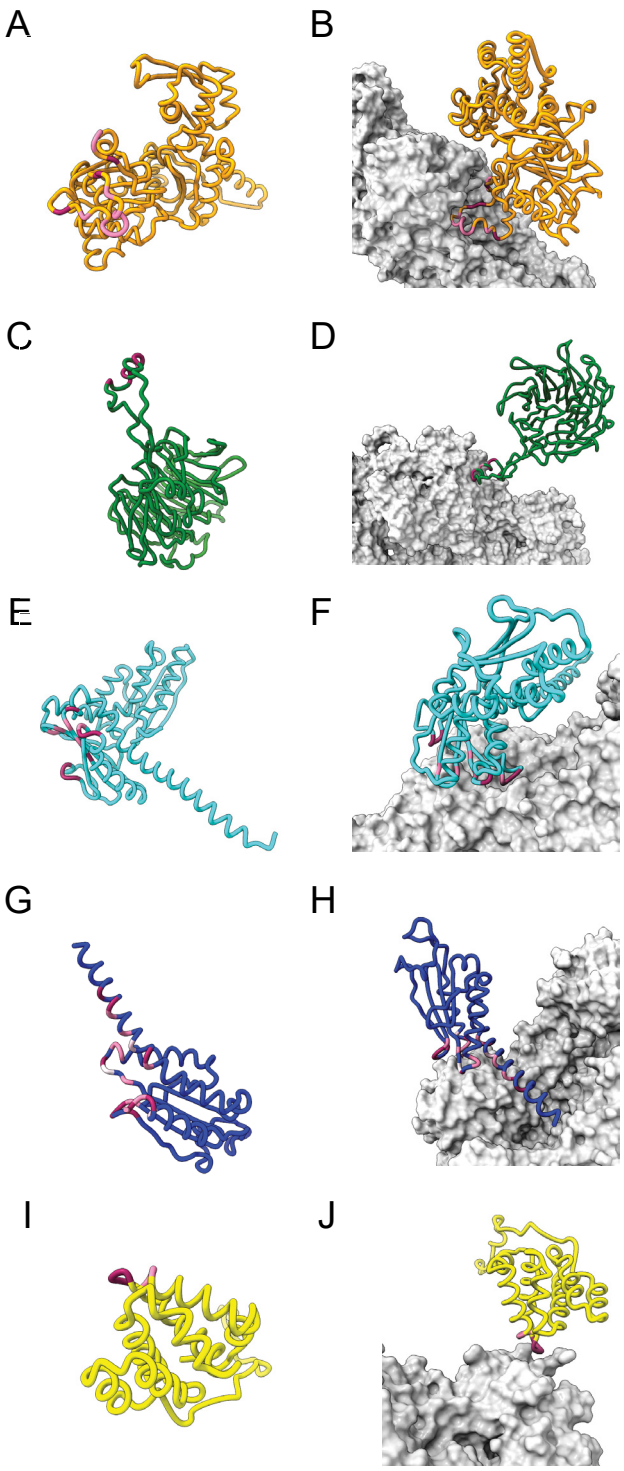

Figure 4.4. Rosetta designed mutations on Arp2/3 complex subunits. Predicted mutation sites are mapped onto individual subunits at the mother filament interface: Arp3 (A-B), ARPC1(C-D), ARPC2 (E-F), ARPC4 (G-H), ARPC5 (I-J). Residues are colored by conservation between models (dark magenta: frequently mutated/less conserved, white: rarely mutated/more conserved). PDB: 4jd2.

Discussion

We found that the two intrinsically disordered regions we examined, the Arp3 D-loop and the ARPC2 C terminal tail, were both important for Arp2/3 complex activation; deletion of either region reduced activity in polymerization assays. This role differs from what was previously seen in budding and fission yeast where the Arp3 D-loop was proposed to act as a steric "bumper" during filament binding[68]. Though the presence of the Arp3 D-loop and the ARPC2 C-terminal tail is conserved, their lengths and sequences are not (Figure 4.1), which may lead to differing roles for IDRs across species. The Arp3 D-loop of ScArp2/3 is ~30 and SpArp2/3 ~15 residues longer than their mammalian counterpart. Though the D-loop in both yeast and mammalian Arp2/3 complexes is observed at the interface with the mother filament in branch junction structures, the extra residues may provide the length in the loop that produces the bumper effect[78,79]. Because the loop is shorter in mammalian complexes, a larger portion of the loop was removed in the HsArp2/3 complex which may have impacted its function, whether in filament binding or complex stabilization. The ARPC2 C terminal tail has not been characterized in yeast but also has varying lengths between species, shorter (by ~10 residues) in mammalian and SpArp2/3 complexes than in ScArp2/3 complex. Both IDRs may still have roles in tuning filament binding affinity, acting to decrease it in yeast and increase it in mammals. If the IDRs of mammals don't influence binding affinity, however, they may influence activity through a unique mechanism. Other differences in the mechanisms of Arp2/3 complexes from different species have been observed. For example, phosphorylation influences activity of mammalian Arp2/3 complex, but is less critical in yeast[124,125,157]. Additionally, ScArp2/3 complex has significantly higher basal activity in the absence of nucleation promoting factors. The cytoskeletal networks of humans are more complex environments containing more regulatory

proteins[49,158]. Yeast may require structural elements to provide regulatory functionalities lacking in their simpler cytoskeletal environment.

We set out to design a strengthened filament binding interface, but further analysis of the Rosetta-designed mutations is necessary before purification, screening, and characterization. By selecting the most common mutations and considering the electrostatic and steric consequences of the change in both the inactive and active state of the Arp2/3 complex, we hope to purify a construct that has increased binding affinity without disruption of critical function. This can be difficult to predict as mutations can have confounding effects on the stability of the complex or its activation. Sequence analysis of evolutionary ancestors can be utilized to determine whether introduction of mutations at a specific site retains the stability of the protein[159]. Evaluation of the conservation of residues at the interface may offer additional insight on residues that may be critical for function. Changing a residue may have unintended consequences for activation if activating conformational changes that occur via allostery are affected. The precise mechanisms of activating conformational changes remain unclear, meaning several iterations of purification and characterization are likely needed to produce a functional construct with increased binding affinity for actin filaments. Because of the difficulty in cloning and purifying complexes with several mutations in multiple subunits, it may be worthwhile to focus the design effort on a single subunit guided by the results of the overall protein design.

Methods

Proteins

Actin was purified from rabbit muscle acetone powder and labeled with pyrene

iodoacetamide as previously described[110]. GST-N-WASP-VCA were purified as previously described[120].

The human Arp2/3 complex containing the Arp3A, ARPC1B, and ARPC5L isoforms was expressed using the biGBac insect expression system[136]. Tandem 12x His and TwinStrep tags were added to the C terminus of ARPC1. Cloning and expression of all subunits (Arp2, Arp3, ARPC1, ARPC2, ARPC3, ARPC4, ARPC5) and a fluorescent marker (mNeonGreen) was completed as previously described[149]. Cells were harvested via centrifugation after addition of 1mM phenylmethylsulfonyl fluoride (PMSF) and stored at -80 °C until purification.

Arp2/3 complex was purified by resuspending cell pellets in PKME buffer (25mM PIPES-KOH pH 7, 50 mM KCl, 1 mM EGTA, 3 mM $MgCl_2$, 1 mM dithiothreitol (DTT), 0.1mM ATP) supplemented with cOmplete Mini EDTA-free Protease Inhibitor Cocktail (Roche) and 1.25 U/mL Benzonase Nuclease (Millipore Sigma) and lysing via sonication. Cell lysate was supplemented with 1 mM PMSF and clarified via ultracentrifugation in a Ti70 rotor for one hour at 52k RPM. The filtrate was then loaded on a glutathione Sepharose 4B (Cytiva) GST-N-WASP VCA column prepared as previously described[90], washed with PKME, PKME + 50 mM KCl, and PKME + 100 mM KCl, and then eluted via a 150 mM to 1M NaCl gradient in 20 mM Tris-HCl pH 8 and 1 mM DTT. The elution was diluted to 30 mM NaCl, injected into a Source30Q anion exchange column, and eluted over a linear gradient from 30 mM NaCl to 500 mM NaCl in 20 mM Tris pH 8 and 1 mM DTT. Pure fractions were run over a glutathione Sepharose 4B column to remove any residual GST-N-WASP-VCA before concentration in a stirred ultrafiltration cell (Amicon) with a Hydrosart 30 kDa molecular weight cutoff filter (Sartorius) and injected into a Superdex200 column in 20 mM Tris pH 8 and 600mM NaCl. Pooled fractions from the size exclusion chromatography were concentrated using the stirred ultrafiltration cell,

buffer exchanged to 20 mM Tris pH 8, 100 mM NaCl, and 1 mM DTT, flash frozen, and stored at -80 °C. Concentrations were determined by measuring absorbance at 280 nm (ε_{280}= 237,000 $M^{-1}cm^{-1}$).

Pyrene actin polymerization assays

Pyrene actin polymerization assays were done on a TECAN Safire 2 plate reader with excitation at 365 nm and emission at 407 nm. A 10x solution of M/E buffer (5 mM $MgCl_2$, 20 mM EGTA) was added to rabbit skeletal muscle actin in G buffer (5 mM Tris pH 8.0, 0.2 mM $CaCl_2$, 0.2 mM ATP, 0.2 mM DTT) in a 96-well black flat bottom half-area plate (Corning 3686) and the solution was incubated for 2 minutes. Arp2/3 complex and the indicated proteins were pre-mixed and, when ready to start the reaction, added to the actin at the concentrations indicated. The final reaction consisted of an actin concentration of 3 µM 15% pyrene-labeled actin, and a final buffer composition of 10 mM Imidazole-HCl pH 7.0, 50 mM KCl, 1 mM EGTA, 1 mM $MgCl_2$, 0.2 mM ATP, and 1mM DTT.

Rosetta design

To design the higher affinity HsArp2/3 construct in Rosetta, we prepared a structure starting from the inactive *Bos taurus* (Bt) Arp2/3 complex (PDB: 4jd2). To dock the inactive complex onto an actin filament, we overlaid the structure onto the Arp2/3 complex at a branch junction (PDB: 7tpt). Missing loops were added in ChimeraX using modeler and side chains were completed in ChimeraX using dock prep. Non-conserved residues between Bt and Hs complexes were mutated to the Hs residues in Coot. Clashes were resolved and any changes made were minimized in Coot. Any non-amino acid molecules were removed prior to

renumbering residues in all chains to be sequential, rather than independent. The actin filament was redefined as one chain. This prepared structure was relaxed in Rosetta and checked against the input structure to ensure no large movements had occurred.

The relaxed structure was used to run the design protocol in Rosetta. The FastDesign mover was used alongside the InterfaceAnalyzerMover to evaluate the interface between the filament and Arp2/3 complex. Residues within 8 A° of the actin filament were able to be mutated to any amino acid except Cysteine and moved while mutations and movement of the actin filament itself were restricted. This protocol output 10 design models with multiple mutations in the Arp2/3 complex. Mutations were evaluated by aligning the output sequences and using ConSurf to determine the conservation at each position.

Bridge to Chapter V

In Chapter IV, I demonstrated that perturbations in the Arp2/3 complex interface with the mother actin filament influence its nucleation activity. I found that deletion of intrinsically disordered regions in the human Arp2/3 complex reduces its nucleation activity, contrary to yeast, where deletion of the Arp3 D-loop increased its activity. I also developed a pipeline to design a complex with increased affinity for actin filaments. Characterization of complexes with low and high binding affinity will advance future studies on how filament binding may influence the ability of the Arp2/3 complex to localize during assembly of actin networks. In Chapter V I will summarize the work of the previous three chapters, discuss how these findings expand our knowledge of actin cytoskeleton regulation, and highlight future directions.

CHAPTER FIVE

CONCLUDING REMARKS

Unraveling the mechanisms involved in Arp2/3 complex regulation is critical to understanding the cellular processes driven by branched actin networks, including cell motility and endocytosis[1,2,4,5]. Additionally, force-producing actin networks have roles in disease states, including pathogen infection and cancer. Bacteria or viruses can hijack the machinery of a host's actin cytoskeleton during cell infection, enabling invasion and replication[160]. Actin structures called invadopodium allow tumors to invade surrounding tissues, contributing to cancer metastasis[161]. A deep understanding of branched network assembly within a complex cellular environment requires a foundation of mechanistic knowledge. My work has focused on the role of activators and structural elements in Arp2/3 complex activation and their influence on the functionality of the complex.

In chapter II, my investigation into the role of actin monomers in human Arp2/3 complex activation provided insight into actin nucleus requirements, Arp2/3 complex regulation, and conservation of mechanisms between yeast and humans. The assembly of monomers into a stable oligomer from which elongation proceeds is a critical step in nucleation mechanisms of spontaneously polymerizing filaments, Arp2/3 complex, formins, and tandem WH2 containing proteins. The unique mechanisms of actin assembly by various nucleators are informed by the minimal requirements of nucleus formation. Kinetic modeling of spontaneous nucleation finds that an actin nucleus must be at least a trimer due to the instability of actin dimers[113,121]. My kinetic modeling shows that, though Arp2 and Arp2 template a new filament by mimicking an actin dimer, they are an insufficient nucleus, indicating that the filament nucleus is at least a trimer in branching nucleation, as in spontaneous nucleation. This trimer can be assembled via a

monomer collision step and does not require WASP for recruitment, as previously proposed[74]. Direct monomer recruitment is thus not a general requirement for human Arp2/3 complex activation but is essential specifically for WASP-mediated activation. This conclusion was previously made in studies of the activation mechanism of the *Saccharomyces cerevisiae* Arp2/3 complex, suggesting that the core activation mechanism is conserved between yeast and humans. Further investigations into the mechanism of branch nucleation will be needed to determine the precise role of actin monomers during WASP-mediated activation.

The analysis of endocytic actin networks in chapter III highlights the importance of investigating established regulatory mechanisms of the Arp2/3 complex within the complexity of a cellular environment. Though we did not observe catastrophic defects in endocytosis when expressing constitutively active Arp2/3 complexes, quantification of patch dynamics exposed small perturbations in actin assembly dynamics. This included longer actin lifetimes, increased actin recruitment, increased actin assembly rates, and increased NPF accumulation. These changes suggest that mutant Arp2/3 complexes assemble actin networks with suboptimal architectures. How the structure of mutant-assembled actin network differs from networks assembled by wildtype Arp2/3 complex cannot be elucidated from these quantifications. The increase in total accumulated actin at peak patch intensity may be a consequence of unproductive branch nucleation from NPF independent activity or a result of increased activation of Arp2/3 complex mutants by WASP. Though both possibilities would influence network architecture, cells appear to tolerate a degree of misregulation as actin patches in the splayed interface mutants were successfully internalized at rates similar to wildtype. The presence of multiple regulatory mechanisms likely prevents failed internalization. Mutants with more severe effects *in vitro* may have a lower tolerance and exhibit more catastrophic defects during endocytosis. Supporting this,

Arp2 (A207C) has higher NPF independent activity than Arp2 (F203Y)[126] and showed increased actin accumulation rates during endocytosis. Investigating other regulatory proteins involved in endocytosis and their effects on activity of the Arp2/3 complex may inform how their mechanisms intersect with that of Arp2/3 complex to influence cellular function. Studies in reconstituted polarized networks such as bead motility assays or micropatterned surfaces can bridge the gap between Arp2/3 complex regulation in bulk solution assays and in the complex cellular environment.

Though much work has been completed on WASP-mediated activation of the Arp2/3 complex, less is known about the role of actin filaments. My work in chapter IV focused on how the filament binding step, specifically the binding affinity of Arp2/3 complex for filaments, affects Arp2/3 complex activation. Previous work found that affinity for actin filaments, modulated through conserved structural insertions, influences the degree of nucleation activity[68]. I investigated structural inserts in the human Arp2/3 complex and found that, though the presence of intrinsically disordered regions is conserved, their role in tuning binding affinity is not. Further work will be required to determine what the role of the Arp3 D-loop is in human Arp2/3 complex activation and why this differs from its role as a steric bumper in yeast. Because the ARPC2 C-terminal tail has not been studied in yeast, characterizations will be required to determine its role across species. Additionally, my work on designing a complex with high binding affinity for filaments will allow us to expand upon what we have learned in isotropic networks by providing the tools for investigating the influence of filament binding affinity on function in polarized networks. This will enhance our knowledge of the kinetics of activation, providing insight on spatiotemporal assembly of actin networks, key to regulation of cellular processes.

Overall, my work has deepened our understanding of the regulation of Arp2/3 complex and highlighted the importance of connecting mechanisms to cellular function. Future work will be needed to clarify the role of actin monomers in WASP-mediated activation of Arp2/3 complex, probe the regulatory mechanisms counteracting misregulation in cells, and investigate how Arp2/3 complex tunes its binding affinity for optimal functionality in polarized networks.

APPENDIX

SUPPLEMENTARY INFORMATION FOR CHAPTER II

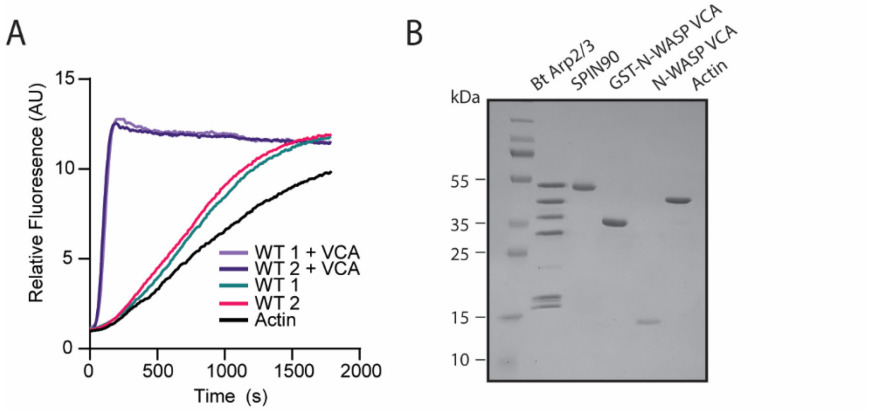

Figure S2.1. Arp2/3 purification yields pure Arp2/3 complex with minimal prep-to-prep variation.
(A) Pyrene actin polymerization time courses comparing activities of WT Arp2/3 complex from different preparations. Reactions contained 3 µM 15% pyrene labeled actin and 50 nM wild-type Arp2/3 complex, with or without 100 nM N-WASP-VCA .
(B) Coomassie-stained SDS-PAGE gel of proteins used in this study. See main text (Figures 2.1A and 2.1B) for HsArp2/3 constructs.

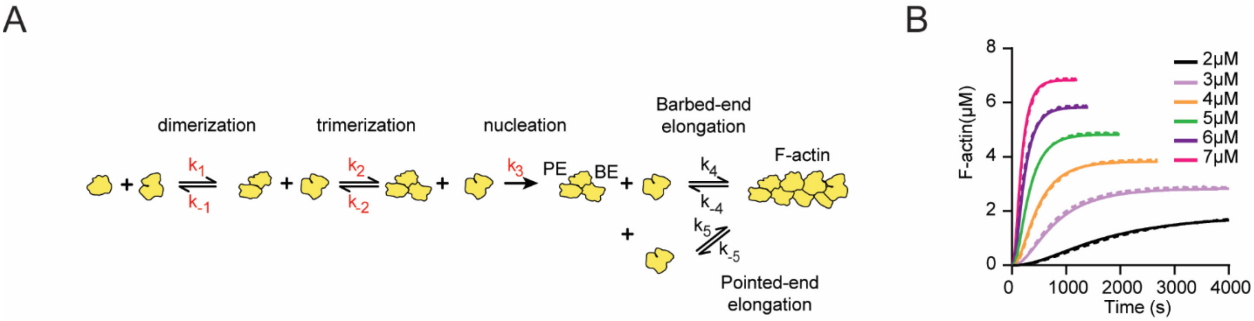

Figure S2.2. Models of spontaneous filament nucleation and elongation.
(A) Pathway of spontaneous filament nucleation and elongation used in mathematical modeling. Floated rate constants are in red and fixed or constrained rate constants (see main text) are in black.
(B) Polymerization time courses (dashed lines) of 15 % pyrene labeled at the indicated concentrations. Best fits from the spontaneous nucleation model in (A) are shown as solid lines.

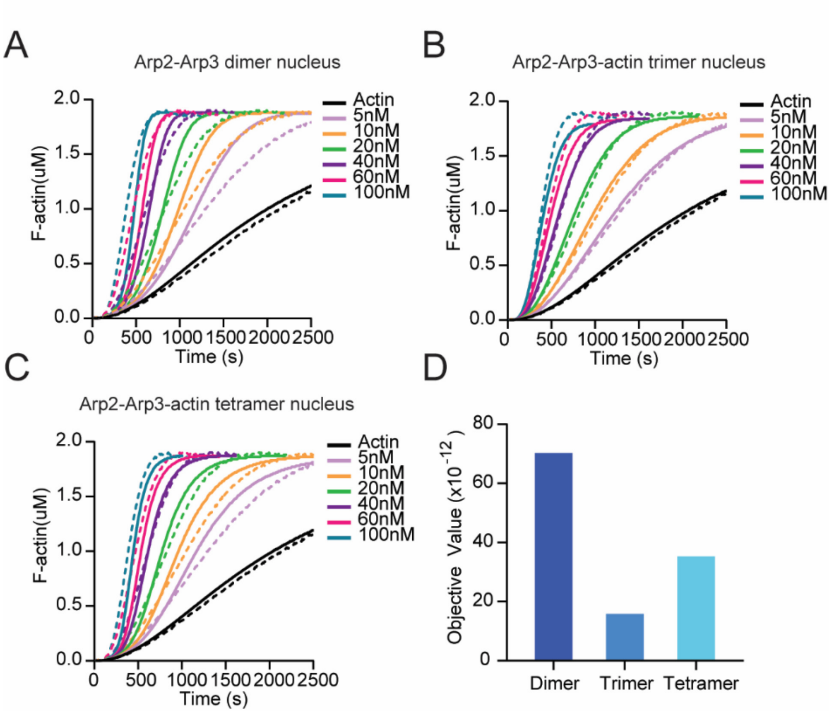

Figure S2.3. The Arp2(F204Y) complex likely requires monomer collision for WASP-independent nucleation.
(A) Polymerization time courses (dashed lines) of 15 % 2 μM pyrene labeled actin with the indicated concentrations of the Arp2(F204Y) complex. Best fits from Model 1 (Arp2-Arp3 dimer nucleus model) simulations are shown as solid lines.
(B) Polymerization time courses as described in (A). Best fits from Model 2 (Arp2-Arp3-actin trimer nucleus model) simulations are shown as solid lines.
(C) Polymerization time courses as described in (A). Best fits from Model 3 (Arp2-Arp3-actin^2 tetramer nucleus model) simulations are shown as solid lines.
(D) Objective values of the best fits from Model 1-3. Objective value is the result of minimization of the normalized weighted sum of squares (see methods).

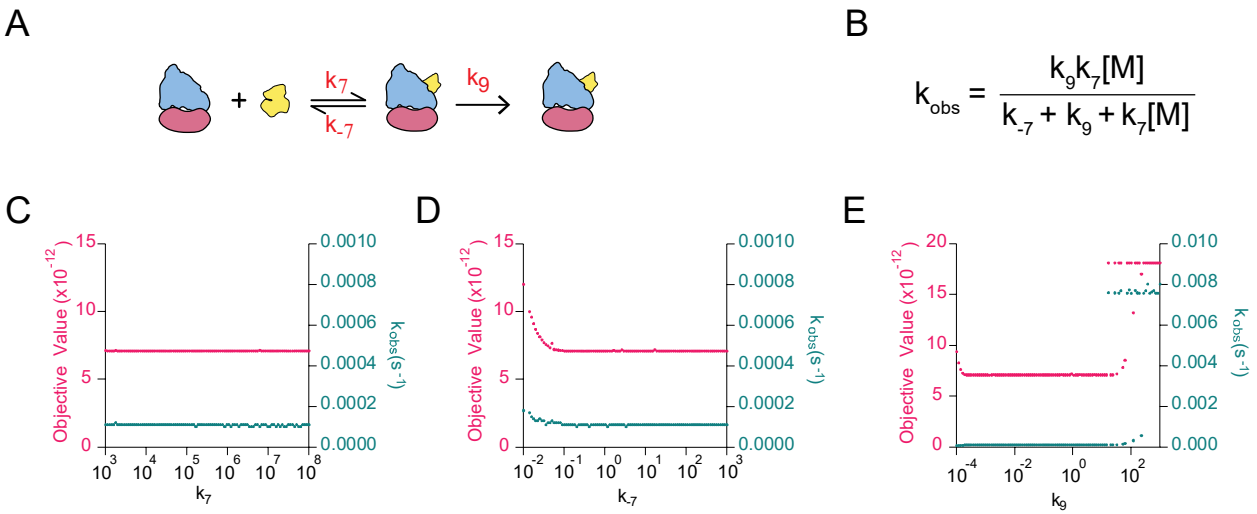

Figure S2.4. The macroscopic rate constant $k_{obs,S90}$ is well determined.
(A) Schematic describing the values used to determine the rate of formation of new ends formed by the SPIN90-Arp2/3 complex, $k_{obs,S90}$.
(B) Derived equation used to calculate $k_{obs,S90}$, defined as the rate of formation of new ends formed by the SPIN90-Arp2/3 complex, as shown in (A). (see methods)
(C) Scan of k_7 values plotted against the resulting objective value in magenta and the calculated $k_{obs,S90}$ in teal.
(D) Scan of k_{-7} values plotted against the resulting objective value in magenta and the calculated $k_{obs,S90}$ in teal.
(E) Scan of k_9 values plotted against the resulting objective value in magenta and the calculated $k_{obs,S90}$ in teal.

A

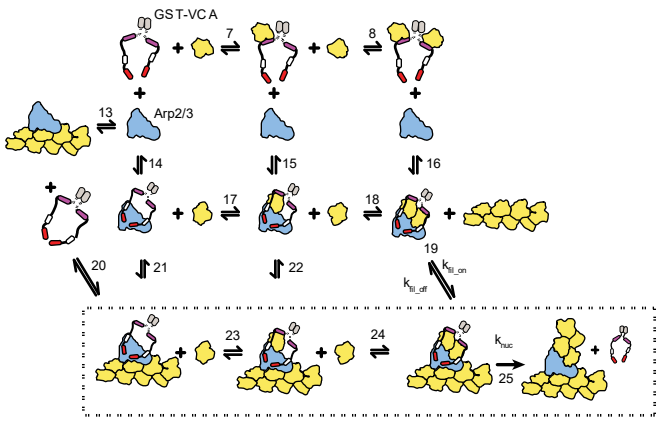

B

$$k_{obs} = \frac{k_{25}k_{23}k_{24}[M]^2}{k_{-23}k_{-24} + k_{-23}k_{25} + k_{23}k_{25}[M] + k_{23}k_{24}[M]^2}$$

Figure S2.5. Determination of the macroscopic rate constant $k_{obs,WASP}$.
(A) Schematic of the WASP-mediated nucleation pathway adapted from Helgeson et al[129]. Dashed box indicates pathway and values used to determine the rate of formation of new ends formed by the WASP-filament-Arp2/3 complex, $k_{obs,WASP,}$
(B) Derived equation used to calculate $k_{obs,WASP,}$ defined as the rate of formation of new ends formed by the WASP-filament-Arp2/3 complex, as shown in (A). (see methods)

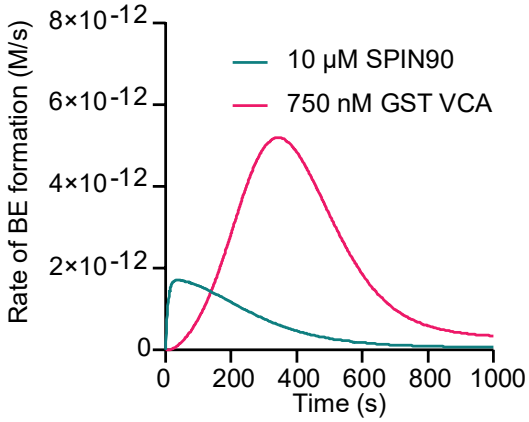

Figure S2.6. Comparison of barbed end formation rates during SPIN90 and WASP-mediated nucleation.
Simulated rates of barbed end formation at saturating concentrations of SPIN90 in teal and GST-VCA in magenta using rates determined from modeling in Figure 2.4 and Helgeson et al[129].

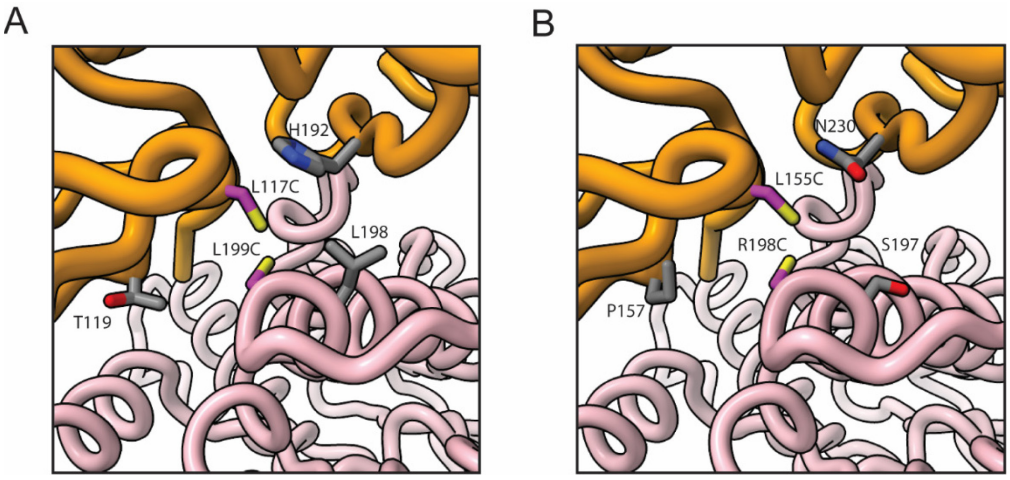

Figure S2.7. Comparison of residues near crosslinked cysteines in mammalian and ScArp2/3 complex.
(A) Non-conserved residues (gray) near crosslinked cysteines (magenta) in BtArp2/3 complex (PDB: 7tpt)
(B) Non-conserved residues (gray) near crosslinked cysteines (magenta) in homology model of ScArp2/3 complex.

Reaction #	Description	k_{on}(M^{-1} s^{-1})	k_{off} (s^{-1})	K_D (μM)	Reference
1	Actin dimerization	3.4*	0.07*	2.19 x 10^4	This Study
2	Actin trimerization	1.20 x 10^3*	13.2*	1.10 x 10^4	This Study
3	Actin trimer nucleation	(1) 9.44E x 10^5*,† (2) 8.87E x 10^5*,† (3) 8.86E x10^5*,†			This Study
4	Barbed end elongation	1.16 x 10^7**	1.4**	0.12	[35]
5	Pointed end elongation	1.3 x 10^6**	0.8**	0.62	[35]
6	A208W binds filament	(1) 3.62 x 10^6 (2) 8.65 x 10^6 (3) 3.37 x 10^6	6.51* 15.6* 6.06*	1.8**	This study, [72,74]
7	Actin monomer binds A208W – filament	(2) 1.01 x 10^6* (3) 8.75 x 10^3*	0.2* 46.5*	0.19 5.31 x 10^3	This Study
8	Actin monomer binds A208W - filament – monomer	(3) 1.33 x 10^5*	0.2*	4.97 x 10^{-2}	This Study
9	A208W nucleation	(1) 5.59 x 10^{-5}*,† (2) 1.55 x 10^{-5}*,† (3) 3.94 x 10^5*,†			This Study

* indicates floated parameters
** indicates fixed parameters
† Units are s^{-1}

Table S2.1. Rate constants determined from mathematical modeling of A208W nucleation. Values determined from mathematical modeling in Figures 2.3 and S2.2, or previously determined in referenced studies. Model numbers are listed for values specific to a model.

Reaction #	Description	k_{on}(M^{-1} s^{-1})	k_{off} (s^{-1})	K_D (µM)	Reference
1	Actin dimerization	3.4*	0.07*	2.19×10^4	This Study
2	Actin trimerization	1.20×10^3*	13.2*	1.10×10^4	This Study
3	Actin trimer nucleation	(1) 8.00×10^5*,† (2) 7.53×10^5*,† (3) 7.68×10^5*,†			This Study
4	Barbed end elongation	1.16×10^7**	1.4**	0.12	[35]
5	Pointed end elongation	1.3×10^6**	0.8**	0.62	[35]
6	F204Y binds filament	(1) 1.14×10^7 (2) 3.99×10^7 (3) 2.67×10^7	20.53* 71.8* 48*	1.8**	This Study
7	Actin monomer binds F204Y - filament	(2) 3.76×10^7* (3) 6.15×10^5*	0.57* 163*	1.45×10^3 7.81×10^3	This Study
8	Actin monomer binds F204Y - filament - monomer	(3) 4.84×10^7*	144*	2.98	This Study
9	F204Y nucleation	(1) 1.61×10^{-4}*,† (2) 1.49×10^{-5}*,† (3) 5.05×10^{-2}*,†			This Study

* indicates floated parameters
** indicates fixed parameters
† Units are s^{-1}

Table S2.2. Rate constants determined from mathematical modeling of F204Y nucleation. Values determined from mathematical modeling in Figures S2.2 and S2.3, or previously determined in referenced studies. Model numbers are listed for values specific to a model.

Reaction #	Description	k_{on} (M^{-1} s^{-1})	k_{off} (s^{-1})	K_D (μM)	Reference
1	Actin dimerization	7.78×10^{-2}*	0.66*	8.53×10^{6}	This Study
2	Actin trimerization	1.25×10^{5}*	251*	2.00×10^{3}	This Study
3	Actin trimer nucleation	1.42×10^{9}*,†			This Study
4	Barbed end elongation	1.16×10^{7}**	1.4**	0.12	[35]
5	Pointed end elongation	1.3×10^{6}**	0.8**	0.62	[35]
6	SPIN90 binds Arp2/3	(A) 1.36×10^{6} (B) 8.88×10^{3} (C) 2.75×10^{4}	9.45* 0.05* 0.19*	6.96*** 6.17*** 6.91***	This Study
7	Actin monomer binds SPIN90 -Arp2/3	(B) 6.17×10^{4}* (C) 2.22×10^{3}*	89.5* 17.4*	1.45×10^{3} 7.81×10^{3}	This Study
8	Actin monomer binds SPIN90 -Arp2/3-monomer	(C) 2.08×10^{5}*	0.01*	4.97×10^{-2}	This Study
9	SPIN90-bound Arp2/3 nucleation	(A) 9.32×10^{-5}*,† (B) 5.33×10^{-2}*,† (C) 1.95×10^{-2}*,†			This Study

† Units are s^{-1}
* indicates floated parameters
** indicates fixed parameters
*** indicates fixed parameter range

Table S2.3. Rate constants determined from mathematical modeling of SPIN90 activation
Values determined from mathematical modeling in Figures 2.4 and S2.2, or previously determined in referenced studies. Model letters are listed for values specific to a model.

References

1. Goode, B. L., Eskin, J. A. & Wendland, B. Actin and Endocytosis in Budding Yeast. Genetics 199, 315–358 (2015).

2. Chakrabarti, R., Lee, M. & Higgs, H. N. Multiple roles for actin in secretory and endocytic pathways. Curr Biol 31, R603–R618 (2021).

3. Campellone, K. G., Lebek, N. M. & King, V. L. Branching out in different directions: Emerging cellular functions for the Arp2/3 complex and WASP-family actin nucleation factors. Eur J Cell Biol 102, 151301 (2023).

4. Swaney, K. F. & Li, R. Function and regulation of the Arp2/3 complex during cell migration in diverse environments. Curr Opin Cell Biol 42, 63–72 (2016).

5. Blanchoin, L., Boujemaa-Paterski, R., Sykes, C. & Plastino, J. Actin Dynamics, Architecture, and Mechanics in Cell Motility. Physiological Reviews 94, 235–263 (2014).

6. Martin, E. & Suzanne, M. Functions of Arp2/3 Complex in the Dynamics of Epithelial Tissues. Front Cell Dev Biol 10, 886288 (2022).

7. Fletcher, D. A. & Mullins, R. D. Cell mechanics and the cytoskeleton. Nature 463, 485–492 (2010).

8. Hohmann, T. & Dehghani, F. The Cytoskeleton—A Complex Interacting Meshwork. Cells 8, 362 (2019).

9. Lecuit, T. & Lenne, P.-F. Cell surface mechanics and the control of cell shape, tissue patterns and morphogenesis. Nat Rev Mol Cell Biol 8, 633–644 (2007).

10. Chugh, P. et al. Actin cortex architecture regulates cell surface tension. Nat Cell Biol 19, 689–697 (2017).

11. Kelkar, M., Bohec, P. & Charras, G. Mechanics of the cellular actin cortex: From signalling to shape change. Current Opinion in Cell Biology 66, 69–78 (2020).

12. Ennomani, H. et al. Architecture and Connectivity Govern Actin Network Contractility. Curr Biol 26, 616–626 (2016).

13. Pimm, M. L. & Henty-Ridilla, J. L. New twists in actin–microtubule interactions. Mol Biol Cell 32, 211–217 (2021).

14. Quiogue, A. R., Sumiyoshi, E., Fries, A., Chuang, C.-H. & Bowerman, B. Microtubules oppose cortical actomyosin-driven membrane ingression during C. elegans meiosis I polar body extrusion. PLoS Genet 19, e1010984 (2023).

15. Pollard, T. D., Blanchoin, L. & Mullins, R. D. Molecular mechanisms controlling actin filament dynamics in nonmuscle cells. Annu Rev Biophys Biomol Struct 29, 545–576 (2000).

16. Koestler, S. A. et al. F- and G-Actin Concentrations in Lamellipodia of Moving Cells. PLOS ONE 4, e4810 (2009).

17. Abraham, V. C., Krishnamurthi, V., Taylor, D. L. & Lanni, F. The Actin-Based Nanomachine at the Leading Edge of Migrating Cells. Biophysical Journal 77, 1721–1732 (1999).

18. Aroush, D. R.-B. et al. Actin turnover in lamellipodial fragments. Curr Biol 27, 2963-2973.e14 (2017).

19. Höglund, A. S., Karlsson, R., Arro, E., Fredriksson, B. A. & Lindberg, U. Visualization of the peripheral weave of microfilaments in glia cells. J Muscle Res Cell Motil 1, 127–146 (1980).

20. Iwasa, J. H. & Mullins, R. D. Spatial and Temporal Relationships between Actin-Filament Nucleation, Capping, and Disassembly. Current Biology 17, 395–406 (2007).

21. Footer, M. J., Kerssemakers, J. W. J., Theriot, J. A. & Dogterom, M. Direct measurement of force generation by actin filament polymerization using an optical trap. Proceedings of the National Academy of Sciences 104, 2181–2186 (2007).

22. Kovar, D. R. & Pollard, T. D. Insertional assembly of actin filament barbed ends in association with formins produces piconewton forces. PNAS 101, 14725–14730 (2004).

23. Prass, M., Jacobson, K., Mogilner, A. & Radmacher, M. Direct measurement of the lamellipodial protrusive force in a migrating cell. J Cell Biol 174, 767–772 (2006).

24. Mueller, J. et al. Load Adaptation of Lamellipodial Actin Networks. Cell 171, 188-200.e16 (2017).

25. Akamatsu, M. et al. Principles of self-organization and load adaptation by the actin cytoskeleton during clathrin-mediated endocytosis. eLife 9, e49840 (2020).

26. Mund, M. et al. Systematic Nanoscale Analysis of Endocytosis Links Efficient Vesicle Formation to Patterned Actin Nucleation. Cell 174, 884-896.e17 (2018).

27. Jin, M. et al. Branched actin networks are organized for asymmetric force production during clathrin-mediated endocytosis in mammalian cells. Nat Commun 13, 3578 (2022).

28. Dmitrieff, S. & Nédélec, F. Amplification of actin polymerization forces. Journal of Cell Biology 212, 763–766 (2016).

29. Gallop, J. L. Filopodia and their links with membrane traffic and cell adhesion. Seminars in Cell & Developmental Biology 102, 81–89 (2020).

30. Kabsch, W., Mannherz, H. G., Suck, D., Pai, E. F. & Holmes, K. C. Atomic structure of the actin:DNase I complex. Nature 347, 37–44 (1990).

31. Atomic structure of the actin: DNase I complex | Nature. https://www.nature.com/articles/347037a0.

32. Holmes, K. C., Popp, D., Gebhard, W. & Kabsch, W. Atomic model of the actin filament. Nature 347, 44–49 (1990).

33. Oda, T., Iwasa, M., Aihara, T., Maéda, Y. & Narita, A. The nature of the globular- to fibrous-actin transition. Nature 457, 441–445 (2009).

34. Fujii, T., Iwane, A. H., Yanagida, T. & Namba, K. Direct visualization of secondary structures of F-actin by electron cryomicroscopy. Nature 467, 724–728 (2010).

35. Pollard, T. D. Rate constants for the reactions of ATP- and ADP-actin with the ends of actin filaments. Journal of Cell Biology 103, 2747–2754 (1986).

36. Sept, D. & McCammon, J. A. Thermodynamics and kinetics of actin filament nucleation. Biophys J 81, 667–674 (2001).

37. Breitsprecher, D. & Goode, B. L. Formins at a glance. J Cell Sci 126, 1–7 (2013).

38. Pring, M., Evangelista, M., Boone, C., Yang, C. & Zigmond, S. H. Mechanism of Formin-Induced Nucleation of Actin Filaments. Biochemistry 42, 486–496 (2003).

39. Heimsath, E. G. & Higgs, H. N. The C terminus of formin FMNL3 accelerates actin polymerization and contains a WH2 domain-like sequence that binds both monomers and filament barbed ends. J Biol Chem 287, 3087–3098 (2012).

40. Gould, C. J. et al. The formin DAD domain plays dual roles in autoinhibition and actin nucleation. Curr Biol 21, 384–390 (2011).

41. Zuchero, J. B., Coutts, A. S., Quinlan, M. E., La Thangue, N. B. & Mullins, R. D. p53-cofactor JMY is a Multifunctional Actin Nucleation Factor. Nat Cell Biol 11, 451–459 (2009).

42. Quinlan, M. E., Heuser, J. E., Kerkhoff, E. & Dyche Mullins, R. Drosophila Spire is an actin nucleation factor. Nature 433, 382–388 (2005).

43. Ahuja, R. et al. Cordon-Bleu Is an Actin Nucleation Factor and Controls Neuronal Morphology. Cell 131, 337–350 (2007).

44. Chesarone, M. A. & Goode, B. L. Actin nucleation and elongation factors: mechanisms and interplay. Curr Opin Cell Biol 21, 28–37 (2009).

45. Wagner, A. R., Luan, Q., Liu, S.-L. & Nolen, B. J. Dip1 defines a class of Arp2/3 complex activators that function without preformed actin filaments. Curr. Biol. 23, 1990–1998 (2013).

46. Skau, C. T. & Waterman, C. M. Specification of Architecture and Function of Actin Structures by Actin Nucleation Factors. Annu Rev Biophys 44, 285–310 (2015).

47. Mullins, R. D., Stafford, W. F. & Pollard, T. D. Structure, subunit topology, and actin-binding activity of the Arp2/3 complex from Acanthamoeba. J Cell Biol 136, 331–343 (1997).

48. Mullins, R. D., Kelleher, J. F., Xu, J. & Pollard, T. D. Arp2/3 Complex from Acanthamoeba Binds Profilin and Cross-links Actin Filaments. Mol Biol Cell 9, 841–852 (1998).

49. Velle, K. B., Swafford, A. J. M., Garner, E. & Fritz-Laylin, L. K. Actin network evolution as a key driver of eukaryotic diversification. J Cell Sci 137, jcs261660 (2024).

50. Winter, D., Podtelejnikov, A. V., Mann, M. & Li, R. The complex containing actin-related proteins Arp2 and Arp3 is required for the motility and integrity of yeast actin patches. Curr Biol 7, 519–529 (1997).

51. Morrell, J. L., Morphew, M. & Gould, K. L. A Mutant of Arp2p Causes Partial Disassembly of the Arp2/3 Complex and Loss of Cortical Actin Function in Fission Yeast. MBoC 10, 4201–4215 (1999).

52. Nolen, B. J. & Pollard, T. D. Structure and Biochemical Properties of Fission Yeast Arp2/3 Complex Lacking the Arp2 Subunit. J Biol Chem 283, 26490–26498 (2008).

53. Robinson, R. C. et al. Crystal structure of Arp2/3 complex. Science 294, 1679–1684 (2001).

54. Lees-Miller, J. P., Henry, G. & Helfman, D. M. Identification of act2, an essential gene in the fission yeast Schizosaccharomyces pombe that encodes a protein related to actin. Proceedings of the National Academy of Sciences 89, 80–83 (1992).

55. Winter, D. C., Choe, E. Y. & Li, R. Genetic dissection of the budding yeast Arp2/3 complex: A comparison of the in vivo and structural roles of individual subunits. Proceedings of the National Academy of Sciences 96, 7288–7293 (1999).

56. Dimchev, V. et al. Induced Arp2/3 Complex Depletion Increases FMNL2/3 Formin Expression and Filopodia Formation. Frontiers in Cell and Developmental Biology 9, (2021).

57. Wu, C. et al. Arp2/3 Is Critical for Lamellipodia and Response to Extracellular Matrix Cues but Is Dispensable for Chemotaxis. Cell 148, 973–987 (2012).

58. Rogers, S. L., Wiedemann, U., Stuurman, N. & Vale, R. D. Molecular requirements for actin-based lamella formation in Drosophila S2 cells. Journal of Cell Biology 162, 1079–1088 (2003).

59. Svitkina, T. M., Verkhovsky, A. B., McQuade, K. M. & Borisy, G. G. Analysis of the Actin–Myosin II System in Fish Epidermal Keratocytes: Mechanism of Cell Body Translocation. J Cell Biol 139, 397–415 (1997).

60. Svitkina, T. M. & Borisy, G. G. Arp2/3 Complex and Actin Depolymerizing Factor/Cofilin in Dendritic Organization and Treadmilling of Actin Filament Array in Lamellipodia. J Cell Biol 145, 1009–1026 (1999).

61. Yang, C. et al. Actin polymerization promotes invagination of flat clathrin-coated lattices in mammalian cells by pushing at lattice edges. Nat Commun 13, 6127 (2022).

62. Kaksonen, M., Sun, Y. & Drubin, D. G. A Pathway for Association of Receptors, Adaptors, and Actin during Endocytic Internalization. Cell 115, 475–487 (2003).

63. Moreau, V., Galan, J. M., Devilliers, G., Haguenauer-Tsapis, R. & Winsor, B. The yeast actin-related protein Arp2p is required for the internalization step of endocytosis. Mol Biol Cell 8, 1361–1375 (1997).

64. Efimova, N. & Svitkina, T. M. Branched actin networks push against each other at adherens junctions to maintain cell–cell adhesion. J Cell Biol 217, 1827–1845 (2018).

65. Schrank, B. R. et al. Nuclear ARP2/3 drives DNA break clustering for homology-directed repair. Nature 559, 61–66 (2018).

66. Mullins, R. D., Heuser, J. A. & Pollard, T. D. The interaction of Arp2/3 complex with actin: Nucleation, high affinity pointed end capping, and formation of branching networks of filaments. PNAS 95, 6181–6186 (1998).

67. Kelleher, J. F., Atkinson, S. J. & Pollard, T. D. Sequences, structural models, and cellular localization of the actin-related proteins Arp2 and Arp3 from Acanthamoeba. J Cell Biol 131, 385–397 (1995).

68. Liu, S.-L., May, J. R., Helgeson, L. A. & Nolen, B. J. Insertions within the actin core of actin-related protein 3 (Arp3) modulate branching nucleation by Arp2/3 complex. J Biol Chem 288, 487–497 (2013).

69. Rodnick-Smith, M., Liu, S.-L., Balzer, C. J., Luan, Q. & Nolen, B. J. Identification of an ATP-controlled allosteric switch that controls actin filament nucleation by Arp2/3 complex. Nature Communications 7, 12226 (2016).

70. Rodnick-Smith, M., Luan, Q., Liu, S.-L. & Nolen, B. J. Role and structural mechanism of WASP-triggered conformational changes in branched actin filament nucleation by Arp2/3 complex. Proc Natl Acad Sci USA 113, E3834–E3843 (2016).

71. Xu, X.-P. et al. Three-dimensional reconstructions of Arp2/3 complex with bound nucleation promoting factors. The EMBO Journal 31, 236–247 (2012).

72. Goley, E. D., Rodenbusch, S. E., Martin, A. C. & Welch, M. D. Critical Conformational Changes in the Arp2/3 Complex Are Induced by Nucleotide and Nucleation Promoting Factor. Molecular Cell 16, 269–279 (2004).

73. Espinoza Sanchez, Sofia, Metskas, Lauren Ann, Chou, Steven Z., Rhoades, Elizabeth & Pollard, Thomas D. Conformational changes in Arp2/3 complex induced by ATP, WASp-VCA and actin filaments. PNAS https://doi.org/10.1073/pnas.1717594115 (2018) doi:10.1073/pnas.1717594115.

74. Zimmet, A. et al. Cryo-EM structure of NPF-bound human Arp2/3 complex and activation mechanism. Sci Adv 6, eaaz7651 (2020).

75. Rouiller, I. et al. The structural basis of actin filament branching by the Arp2/3 complex. J Cell Biol 180, 887–895 (2008).

76. Shaaban, M., Nolen, B. J. & Chowdhury, S. Cryo-EM reveals the transition of Arp2/3 complex from inactive to nucleation-competent state. Nature Structural & Molecular Biology 27, 1009–1016 (2020).

77. Chou, S. Z., Chatterjee, M. & Pollard, T. D. Mechanism of actin filament branch formation by Arp2/3 complex revealed by a high-resolution cryo-EM structureof the branch junction. Proceedings of the National Academy of Sciences 119, e2206722119 (2022).

78. Ding, B. et al. Structure of Arp2/3 complex at a branched actin filament junction resolved by single-particle cryo-electron microscopy. Proc Natl Acad Sci U S A 119, e2202723119 (2022).

79. Chavali, S. S. et al. Cryo-EM structures reveal how phosphate release from Arp3 weakens actin filament branches formed by Arp2/3 complex. Nat Commun 15, 2059 (2024).

80. Fäßler, F., Dimchev, G., Hodirnau, V.-V., Wan, W. & Schur, F. K. M. Cryo-electron tomography structure of Arp2/3 complex in cells reveals new insights into the branch junction. Nat Commun 11, 6437 (2020).

81. Shaaban, M., Chowdhury, S. & Nolen, B. J. Cryo-EM reveals the transition of Arp2/3 complex from inactive to nucleation-competent state. Nat. Struct. Mol. Biol. https://doi.org/10.1038/s41594-020-0481-x (2020) doi:10.1038/s41594-020-0481-x.

82. Ding, B. et al. Structure of Arp2/3 complex at a branched actin filament junction resolved by single-particle cryo-electron microscopy. Proceedings of the National Academy of Sciences 119, e2202723119 (2022).

83. Le Clainche, C., Pantaloni, D. & Carlier, M.-F. ATP hydrolysis on actin-related protein 2/3 complex causes debranching of dendritic actin arrays. Proc Natl Acad Sci U S A 100, 6337–6342 (2003).

84. Martin, A. C., Welch, M. D. & Drubin, D. G. Arp2/3 ATP hydrolysis-catalysed branch dissociation is critical for endocytic force generation. Nat Cell Biol 8, 826–833 (2006).

85. Marchand, J. B., Kaiser, D. A., Pollard, T. D. & Higgs, H. N. Interaction of WASP/Scar proteins with actin and vertebrate Arp2/3 complex. Nat. Cell Biol. 3, 76–82 (2001).

86. Achard, V. et al. A 'primer'-based mechanism underlies branched actin filament network formation and motility. Curr. Biol. 20, 423–428 (2010).

87. Kramer, D. A., Piper, H. K. & Chen, B. WASP family proteins: Molecular mechanisms and implications in human disease. European Journal of Cell Biology 101, 151244 (2022).

88. Chereau, D. et al. Actin-bound structures of Wiskott–Aldrich syndrome protein (WASP)-homology domain 2 and the implications for filament assembly. Proc Natl Acad Sci U S A 102, 16644–16649 (2005).

89. Higgs, H. N., Blanchoin, L. & Pollard, T. D. Influence of the C Terminus of Wiskott-Aldrich Syndrome Protein (WASp) and the Arp2/3 Complex on Actin Polymerization. Biochemistry 38, 15212–15222 (1999).

90. Tyler, J. J. et al. Phosphorylation of the WH2 domain in yeast Las17/WASP regulates G-actin binding and protein function during endocytosis. Sci Rep 11, 9718 (2021).

91. Ti, S.-C., Jurgenson, C. T., Nolen, B. J. & Pollard, T. D. Structural and biochemical characterization of two binding sites for nucleation-promoting factor WASp-VCA on Arp2/3 complex. Proc. Natl. Acad. Sci. U.S.A. 108, E463-471 (2011).

92. Smith, B. A. et al. Three-color single molecule imaging shows WASP detachment from Arp2/3 complex triggers actin filament branch formation. eLife 2, e01008 (2013).

93. Hetrick, B., Han, M. S., Helgeson, L. A. & Nolen, B. J. Small molecules CK-666 and CK-869 inhibit actin-related protein 2/3 complex by blocking an activating conformational change. Chem. Biol. 20, 701–712 (2013).

94. Papayannopoulos, V. et al. A Polybasic Motif Allows N-WASP to Act as a Sensor of PIP2 Density. Molecular Cell 17, 181–191 (2005).

95. Takenawa, T. & Suetsugu, S. The WASP–WAVE protein network: connecting the membrane to the cytoskeleton. Nat Rev Mol Cell Biol 8, 37–48 (2007).

96. Yarar, D., D'Alessio, J. A., Jeng, R. L. & Welch, M. D. Motility determinants in WASP family proteins. Mol Biol Cell 13, 4045–4059 (2002).

97. Mullins, R. D., Bieling, P. & Fletcher, D. A. From solution to surface to filament: actin flux into branched networks. Biophys Rev 10, 1537–1551 (2018).

98. Funk, J. et al. A barbed end interference mechanism reveals how capping protein promotes nucleation in branched actin networks. Nat Commun 12, 5329 (2021).

99. Uruno, T. et al. Activation of Arp2/3 complex-mediated actin polymerization by cortactin. Nat Cell Biol 3, 259–266 (2001).

100. Guo, S. et al. Abp1 promotes Arp2/3 complex-dependent actin nucleation and stabilizes branch junctions by antagonizing GMF. Nat Commun 9, 2895 (2018).

101. Duncan, M. C., Cope, M. J., Goode, B. L., Wendland, B. & Drubin, D. G. Yeast Eps15-like endocytic protein, Pan1p, activates the Arp2/3 complex. Nat Cell Biol 3, 687–690 (2001).

102. Goley, E. D. & Welch, M. D. The ARP2/3 complex: an actin nucleator comes of age. Nature Reviews Molecular Cell Biology 7, 713–726 (2006).

103. Fregoso, F. E. et al. Mechanism of synergistic activation of Arp2/3 complex by cortactin and WASP-family proteins. Nat Commun 14, 6894 (2023).

104. Helgeson, L. A. & Nolen, B. J. Mechanism of synergistic activation of Arp2/3 complex by cortactin and N-WASP. Elife 2, e00884 (2013).

105. Weaver, A. M. et al. Cortactin promotes and stabilizes Arp2/3-induced actin filament network formation. Curr Biol 11, 370–374 (2001).

106. Liu, T. et al. Cortactin stabilizes actin branches by bridging activated Arp2/3 to its nucleated actin filament. Nat Struct Mol Biol 31, 801–809 (2024).

107. Narvaez-Ortiz, H. Y. & Nolen, B. J. Unconcerted conformational changes in Arp2/3 complex integrate multiple activating signals to assemble functional actin networks. Curr Biol S0960-9822(22)00015-X (2022) doi:10.1016/j.cub.2022.01.004.

108. Liu, S.-L., Helgeson, L. A. & Nolen, B. J. Structure of the nucleation-promoting factor SPIN90 bound to the actin filament nucleator Arp2/3 complex. The EMBO Journal 37, e100005 (2018).

109. Balzer, C. J., Wagner, A. R., Helgeson, L. A. & Nolen, B. J. Single-Turnover Activation of Arp2/3 Complex by Dip1 May Balance Nucleation of Linear versus Branched Actin Filaments. Current Biology 29, 3331-3338.e7 (2019).

110. Balzer, C. J. et al. Synergy between Wsp1 and Dip1 may initiate assembly of endocytic actin networks. eLife 9, e60419 (2020).

111. Liu, T. et al. Arp2/3-mediated bidirectional actin assembly by SPIN90 dimers in metazoans. Preprint at https://doi.org/10.1101/2025.01.31.635869 (2025).

112. Francis, J. et al. Activation of Arp2/3 complex by a SPIN90 dimer in linear actin-filament nucleation. Nat Struct Mol Biol 32, 2272–2284 (2025).

113. Sept, D. & McCammon, J. A. Thermodynamics and kinetics of actin filament nucleation. Biophys. J. 81, 667–674 (2001).

114. Campellone, K. G. & Welch, M. D. A nucleator arms race: cellular control of actin assembly. Nat. Rev. Mol. Cell Biol. 11, 237–251 (2010).

115. Siton-Mendelson, O. & Bernheim-Groswasser, A. Functional Actin Networks under Construction: The Cooperative Action of Actin Nucleation and Elongation Factors. Trends in Biochemical Sciences 42, 414–430 (2017).

116. Rohatgi, R. et al. The interaction between N-WASP and the Arp2/3 complex links Cdc42-dependent signals to actin assembly. Cell 97, 221–231 (1999).

117. Padrick, S. B., Doolittle, L. K., Brautigam, C. A., King, D. S. & Rosen, M. K. Arp2/3 complex is bound and activated by two WASP proteins. Proc. Natl. Acad. Sci. U.S.A. 108, E472-479 (2011).

118. Narvaez-Ortiz, H. Y., Lynch, M. J., Liu, S.-L., Fries, A. & Nolen, B. J. Both Las17-binding sites on Arp2/3 complex are important for branching nucleation and assembly of functional endocytic actin networks in S. cerevisiae. J Biol Chem 300, 105766 (2024).

119. Miki, H. & Takenawa, T. Direct binding of the verprolin-homology domain in N-WASP to actin is essential for cytoskeletal reorganization. Biochem Biophys Res Commun 243, 73–78 (1998).

120. Rodnick-Smith, M., Luan, Q., Liu, S.-L. & Nolen, B. J. Role and structural mechanism of WASP-triggered conformational changes in branched actin filament nucleation by Arp2/3 complex. Proc. Natl. Acad. Sci. U.S.A. 113, E3834-3843 (2016).

121. Rosenbloom, A. D., Kovar, E. W., Kovar, D. R., Loew, L. M. & Pollard, T. D. Mechanism of actin filament nucleation. Biophys J 120, 4399–4417 (2021).

122. Dominguez, R. The WH2 Domain and Actin Nucleation: Necessary but Insufficient. Trends Biochem Sci 41, 478–490 (2016).

123. Wen, K.-K. & Rubenstein, P. A. Acceleration of Yeast Actin Polymerization by Yeast Arp2/3 Complex Does Not Require an Arp2/3-activating Protein*. Journal of Biological Chemistry 280, 24168–24174 (2005).

124. LeClaire, L. L., Baumgartner, M., Iwasa, J. H., Mullins, R. D. & Barber, D. L. Phosphorylation of the Arp2/3 complex is necessary to nucleate actin filaments. J. Cell Biol. 182, 647–654 (2008).

125. Epstein, A. E., Espinoza-Sanchez, S. & Pollard, T. D. Phosphorylation of Arp2 is not essential for Arp2/3 complex activity in fission yeast. Life Sci Alliance 1, e201800202 (2018).

126. Rodnick-Smith, M., Liu, S.-L., Balzer, C. J., Luan, Q. & Nolen, B. J. Identification of an ATP-controlled allosteric switch that controls actin filament nucleation by Arp2/3 complex. Nat Commun 7, 12226 (2016).

127. Beltzner, C. C. & Pollard, T. D. Pathway of actin filament branch formation by Arp2/3 complex. J. Biol. Chem. 283, 7135–7144 (2008).

128. Goley, E. D. et al. An actin-filament-binding interface on the Arp2/3 complex is critical for nucleation and branch stability. Proc Natl Acad Sci U S A 107, 8159–8164 (2010).

129. Helgeson, L. A. & Nolen, B. J. Mechanism of synergistic activation of Arp2/3 complex by cortactin and N-WASP. eLife 2, e00884 (2013).

130. Smith, B. A., Daugherty-Clarke, K., Goode, B. L. & Gelles, J. Pathway of actin filament branch formation by Arp2/3 complex revealed by single-molecule imaging. PNAS 110, 1285–1290 (2013).

131. Cao, L., Ghasemi, F., Way, M., Jégou, A. & Romet-Lemonne, G. Regulation of branched versus linear Arp2/3-generated actin filaments. EMBO J 42, e113008 (2023).

132. Weed, S. A. et al. Cortactin Localization to Sites of Actin Assembly in Lamellipodia Requires Interactions with F-Actin and the Arp2/3 Complex. J Cell Biol 151, 29–40 (2000).

133. Helgeson, L. A., Prendergast, J. G., Wagner, A. R., Rodnick-Smith, M. & Nolen, B. J. Interactions with Actin Monomers, Actin Filaments, and Arp2/3 Complex Define the Roles of WASP Family Proteins and Cortactin in Coordinately Regulating Branched Actin Networks*. Journal of Biological Chemistry 289, 28856–28869 (2014).

134. Green, N. S., Reisler, E. & Houk, K. N. Quantitative evaluation of the lengths of homobifunctional protein cross-linking reagents used as molecular rulers. Protein Sci 10, 1293–1304 (2001).

135. Doolittle, L. K., Rosen, M. K. & Padrick, S. B. Purification of Native Arp2/3 Complex from Bovine Thymus. Methods Mol Biol 1046, 231–250 (2013).

136. Weissmann, F. et al. biGBac enables rapid gene assembly for the expression of large multisubunit protein complexes. Proc Natl Acad Sci USA 113, E2564–E2569 (2016).

137. Abella, J. V. G. et al. Isoform diversity in the Arp2/3 complex determines actin filament dynamics. Nat Cell Biol 18, 76–86 (2016).

138. Hoops, S. et al. COPASI—a COmplex PAthway SImulator. Bioinformatics 22, 3067–3074 (2006).

139. Kaksonen, M. & Roux, A. Mechanisms of clathrin-mediated endocytosis. Nat Rev Mol Cell Biol 19, 313–326 (2018).

140. Weinberg, J. & Drubin, D. G. Clathrin-mediated endocytosis in budding yeast. Trends in Cell Biology 22, 1–13 (2012).

141. Aghamohammadzadeh, S. & Ayscough, K. R. Differential requirements for actin during yeast and mammalian endocytosis. Nat Cell Biol 11, 1039–1042 (2009).

142. Taylor, M. J., Perrais, D. & Merrifield, C. J. A High Precision Survey of the Molecular Dynamics of Mammalian Clathrin-Mediated Endocytosis. PLoS Biol 9, e1000604 (2011).

143. Sun, Y. et al. Direct comparison of clathrin-mediated endocytosis in budding and fission yeast reveals conserved and evolvable features. eLife 8, e50749 (2019).

144. Wang, X., Galletta, B. J., Cooper, J. A. & Carlsson, A. E. Actin-Regulator Feedback Interactions during Endocytosis. Biophys J 110, 1430–1443 (2016).

145. Skau, C. T. & Kovar, D. R. Fimbrin and tropomyosin competition regulates endocytosis and cytokinesis kinetics in fission yeast. Curr Biol 20, 1415–1422 (2010).

146. Cai, L., Makhov, A. M., Schafer, D. A. & Bear, J. E. Coronin 1B antagonizes Cortactin and remodels Arp2/3-containing actin branches in lamellipodia. Cell 134, 828–842 (2008).

147. Kaiser, D. A., Vinson, V. K., Murphy, D. B. & Pollard, T. D. Profilin is predominantly associated with monomeric actin in Acanthamoeba. J Cell Sci 112 (Pt 21), 3779–3790 (1999).

148. Bieling, P. et al. WH2 and proline-rich domains of WASP-family proteins collaborate to accelerate actin filament elongation. The EMBO Journal 37, 102–121 (2018).

149. Carlson, S. R. & Nolen, B. J. Direct actin monomer delivery is a WASP-specific requirement for human Arp2/3 complex activation. Journal of Molecular Biology (2025).

150. Boettner, D. R. et al. The F-BAR Protein Syp1 Negatively Regulates WASp-Arp2/3 Complex Activity during Endocytic Patch Formation. Current Biology 19, 1979–1987 (2009).

151. Luan, Q., Zelter, A., MacCoss, M. J., Davis, T. N. & Nolen, B. J. Identification of Wiskott-Aldrich syndrome protein (WASP) binding sites on the branched actin filament nucleator Arp2/3 complex. Proc Natl Acad Sci USA 115, E1409–E1418 (2018).

152. Daniel Gietz, R. & Woods, R. A. Transformation of yeast by lithium acetate/single-stranded carrier DNA/polyethylene glycol method. in Methods in Enzymology (eds Guthrie, C. & Fink, G. R.) vol. 350 87–96 (Academic Press, 2002).

153. Miura, K. Bleach correction ImageJ plugin for compensating the photobleaching of time-lapse sequences. Preprint at https://doi.org/10.12688/f1000research.27171.1 (2020).

154. Tinevez, J.-Y. et al. TrackMate: An open and extensible platform for single-particle tracking. Methods 115, 80–90 (2017).

155. Pollard, T. D. & Borisy, G. G. Cellular Motility Driven by Assembly and Disassembly of Actin Filaments. Cell 112, 453–465 (2003).

156. Mahaffy, R. E. & Pollard, T. D. Kinetics of the formation and dissociation of actin filament branches mediated by Arp2/3 complex. Biophys J 91, 3519–3528 (2006).

157. Narayanan, A., Iii, L. L. L., Barber, D. L. & Jacobson, M. P. Phosphorylation of the Arp2 Subunit Relieves Auto-inhibitory Interactions for Arp2/3 Complex Activation. PLOS Computational Biology 7, e1002226 (2011).

158. Pollard, T. D. Actin and Actin-Binding Proteins. Cold Spring Harb Perspect Biol 8, a018226 (2016).

159. Listov, D., Goverde, C. A., Correia, B. E. & Fleishman, S. J. Opportunities and challenges in design and optimization of protein function. Nat Rev Mol Cell Biol 25, 639–653 (2024).

160. Welch, M. D. & Way, M. Arp2/3-Mediated Actin-Based Motility: A Tail of Pathogen Abuse. Cell Host & Microbe 14, 242–255 (2013).

161. Molinie, N. & Gautreau, A. The Arp2/3 Regulatory System and Its Deregulation in Cancer. Physiological Reviews 98, 215–238 (2018).